Genomic data improve coalescent inference across a range of demographic parameters and life-histories

Running title: Isolation with migration in sea stars

Michael W. Hart[1] | Vanessa I. Guerra[1,2] | Maria Byrne[3] | Jonathan B. Puritz[4]

[1]Department of Biological Sciences, Simon Fraser University, Burnaby, BC, Canada

[2]Department of Invertebrate Zoology, National Museum of Natural History, Smithsonian Institution, Washington, DC 20013, USA

[3]School of Biological Sciences, University of Sydney, Sydney, NSW, Australia

[4]Department of Biological Sciences, University of Rhode Island, Kingston, RI, USA

Correspondence: Michael Hart. Email: mwhart@sfu.ca

Abstract

Understanding the demographic context for population divergence and speciation in the sea often requires distinguishing the contributions of mutation, isolation, and gene flow on temporal or geographical scales where those diverse processes may not achieve equilibrium conditions. Coalescent isolation-with-migration (IM) models can meet this need for non-equilibrium modelling of genetic variation, but the quality of IM model parameter estimation depends on the breadth of genome sampling. Here, we describe three improvements in IM parameter estimates based on hundreds of loci from RNA-seq assemblies relative to previously published results based on few loci in two sea star study systems that differ in the tempo of population divergence. (1) Precision of all model parameter value estimates (with narrow posterior distributions) was vastly better in both study systems and resolved uncertainty around one key parameter in each. (2) Maximum likelihood estimates of some

model parameters were broadly similar to previously published estimates, but with greater precision we obtained more realistic values for some parameters that were consistent with expectations based on the biogeography of the organisms. (3) We found non-zero but demographically trivial gene flow in one study system where we previously estimated gene flow to be zero, and modest symmetrical gene flow ($2Nm<1$) in a second study system where we previously estimated gene flow to be massive ($2Nm\sim10$) and asymmetrical. Improved understanding through judicious application of genome-wide sampling in replication studies as shown here may improve the information needed for biodiversity management and conservation.

KEYWORDS

Cryptasterina, *Patiria miniata*, Asterinidae, migration, divergence time, replication study

1 | Introduction

Coalescent models of isolation with migration (IM) have played an important role in understanding interactions among evolutionary processes that lead to population structure, spatial differentiation, and reproductive divergence (Pinho & Hey, 2010). Advantages of the IM approach include the potential to model rates of mutation, genetic drift, and migration together in a non-equilibrium context characterized by the times of splitting or divergence between sampled (and unsampled) populations. Modelling those processes together allows their individual contributions to be estimated, and can lead to insights into which specific process(es) might be responsible for observed patterns of spatial structure, and for variation in those patterns across different organisms in different landscapes or seascapes (e.g., Hart & Marko, 2010; Weber et al., 2015; Selkoe et al., 2016; Puritz et al., 2017).

Like some other areas of population genetics analysis, the development of IM models and theory for many years outpaced the development of data collection methods that could fulfill the data requirements for fitting the models. In particular, for the family of coalescent IM models that sample genealogies using Markov chain Monte Carlo optimization methods (Hey & Nielsen, 2004; Hey, 2010a; Sethuraman & Hey, 2016; Hey et al., 2018), model fitting and parameter value estimation depend on broad sampling of many loci across the genome in order to account for the expected variance in coalescent patterns among loci (Edwards & Beerli, 2000; Felsenstein 2006). Before the genomics revolution of the early 21st century, and the democratization of affordable second-generation sequencing technology, the most effective applications of IM methods were limited to model organisms or to species closely related to a model organism for which good genomics resources were available (e.g., Won & Hey, 2005; Hey, 2010b). At the same time, researchers working on non-model organisms also widely adopted these IM methods, but fitted the model parameters to limited datasets derived from labourious and expensive Sanger sequencing of smaller numbers of loci. The costs and benefits of broad genomic sampling with high-throughput methods, and the specific circumstances under which

such sampling might be needed (and the expense might be considered justified), were at that time an active area of debate and discussion. For example, in their review of the role and relative importance of single-locus mtDNA analyses (or "phylogeography unplugged"), Bowen et al. (2014) concluded that "at this stage of technology and software development, judicious rather than wholesale application of genomics appears to be the most robust course for marine phylogeographic studies."

In that context, we published with colleagues a series of comparative phylogeographic studies of asterinid sea stars, based on different combinations of mtDNA haplotypes, microsatellite genotypes, and haplotypes sequenced from small numbers of nuclear genes. Asterinid sea stars are a particularly good model systems for comparative phylogeography because the family is species-rich, phylogenetic relationships are well known, and the adult organisms have similar distributions and natural history (omnivorous grazers or predators in intertidal habitats) (Hart, Byrne, & Smith, 1997; Waters, O'Loughlin, & Roy, 2004), but the larval forms and modes of reproduction are diverse with many instances of parallel or convergent evolution of derived life history traits (Villinski, Byrne, & Raff, 2002; Byrne, 2006). Our general goal in those studies was to understand how the evolution of derived life history traits (including small adult body size, limited planktonic larval duration, nonfeeding larval development, self-fertilization, and viviparous brooding) among some asterinid species and lineages has shaped the evolution of population genetic variation, especially the spatial distribution of genetic diversity and its association with incipient or realized speciation events (Barbosa, Klanten, Puritz, Toonen, & Byrne, 2013; Keever et al., 2009; Keever et al., 2013; McGovern, Keever, Saski, Hart, & Marko, 2010; Puritz et al., 2012; Puritz et al., 2017).

One specific goal of those studies was to understand the historical or demographic context for the evolution of those derived life history traits and phylogeographic patterns. We discovered two surprising temporal patterns of divergence: remarkably recent Holocene divergence between the sister species *Cryptasterina pentagona* (MULLER & TROSCHEL 1840) and *C. hystera* DARTNALL & BYRNE

2003 that have evolved large differences in mating system and fertilization traits in about 6000 years (Puritz et al., 2012); and an unexpectedly old Pleistocene divergence time between conspecific populations of *Patiria miniata* (BRANDT 1835) that have dispersing planktonic larvae and are not expected to evolve a deep, old (280,000 years) phylogeographic break between populations (McGovern et al., 2010). On the basis of those analyses of small samples of loci, we concluded that accounting for the time scale of divergence with gene flow – especially the divergence times between populations or species – forms an important part of understanding the population biology and evolution of these sea stars.

Subsequent technology improvements now make it possible to obtain sequence data in reduced-representation genomes (Davey et al., 2011; Peterson et al., 2012; Toonen et al., 2013), exomes (Puritz & Lotterhos, 2018) or transcriptomes (Cahais et al., 2012) for genome-wide sampling of population genetic variation in analyses of isolation with gene flow in non-model organisms (McCormack et al., 2013; Nadachowska-Brzyska et al., 2013). The incorporation of fast parallel processing methods into IM software now allows IM models to be fit to genome-wide samples of loci with computation times in hours or days (rather than months or years; Sethuraman & Hey, 2016). These technological innovations have created opportunities to learn from past phylogeographic studies about the importance or utility of genome-wide sampling of loci.

Here we use genome-wide sampling from RNA-seq data for gonad transcriptomes in a replication study of two asterinid sea star taxa (McGovern et al., 2010; Puritz et al., 2012) in which we previously reported surprising divergence times associated with the evolution of life history traits including quantitative differences in gamete compatibility between members of diverging populations in *Patiria miniata* (Hart et al., 2014) and qualitative differences in mating system traits between sister species in *Cryptasterina* (Byrne, 2005). In addition to better sampling of the genome in both systems, our new analyses take advantage of better transcriptome assembly methods, isolation-with-migration

104 model improvements (including the resolution of a previously noted software bug that had pernicious
105 effects on parameter value estimates; Hart and Puritz, 2020), and more realistic biogeographic
106 calibrations of mutation rates. All of these improvements have become available since our
107 phylogeographic studies were designed in the "unplugged" era.

108 For both study systems, we sampled many loci from a few individuals from each population;
109 that sampling scheme captures many of the benefits of broad genomic sampling noted by Wang & Hey
110 (2010). We show that analyzing hundreds of loci leads to more precise estimates of isolation-with-
111 migration model parameter values (Felsenstein, 2006). This better precision includes all parameters in
112 both study systems, and resolves some persistent and important ambiguities in our previously published
113 analyses in which small samples of loci contained too little coalescent information to successfully
114 estimate all of the model parameter values. The combination of software improvements and better
115 mutation rate calibrations leads to some changes in estimates of divergence times and effective
116 population sizes, but some of our new estimates based on hundreds of loci differ little from our
117 previously published estimates based on few loci. Many of those differences reflect increased precision
118 associated with better genome sampling, rather than errors in our previous studies and conclusions. The
119 most pronounced and consistent differences involved estimates of gene flow, including non-zero gene
120 flow between species (in *Cryptasterina*, where one species lacks adaptations for dispersal, and where
121 we previously estimated gene flow between species to be zero), and low symmetrical gene flow
122 between populations (in *Patiria miniata*, with long-lived feeding planktonic larvae, where we
123 previously estimated gene flow to be asymmetrical and high in only one direction). Those
124 improvements suggest that many similar study systems from the "unplugged" era might also benefit
125 from replication studies based on fast, cheap, genome-wide sampling of haplotype variation in IM
126 models. Such improvements as generated here can provide important new insight to inform the
127 conservation and management of marine ecosystems.

2 | MATERIALS AND METHODS

2.1 | Two study systems

Cryptasterina hystera and *C. pentagona* are closely-related sister species with adjacent geographic ranges in shallow coastal habitats from the tropical southwestern Pacific near Australia (Dartnall et al,. 2003). Adults of *C. pentagona* are small (radius <2 cm) gonochoric broadcast spawners with planktonic fertilization of large, yolk-rich eggs. Fertilized eggs develop into planktonic larvae that are capable of dispersal and gene flow in ocean currents, followed by settlement and metamorphosis into a benthic juvenile sea star. The northward geographical extent of *C. pentagona* from the coast of southern Queensland to New Guinea (and perhaps beyond) is poorly characterized but consistent with expectations for a species with planktonic larval dispersal. By contrast, adults of *C. hystera* are simultaneous hermaphrodites with internal self-fertilization; embryos and larvae resemble those of *C. pentagona* but develop within the gonad of the parent (rather than in the plankton), followed by metamorphosis to the juvenile form; and juveniles are born live through the gonopores of the parent, without a planktonic stage in the life cycle (Byrne et al., 2003; Byrne, 2005; Byrne, 2006). Populations of *C. hystera* have a highly restricted distribution that includes a short region of the coast of Queensland <100 km south of the southern range limit for *C. pentagona*, plus some atolls of the southern Great Barrier Reef. We previously sequenced PCR amplicons of mtDNA and two nuclear gene introns from both species, and found stark differences in population structure and genetic diversity between species, including extreme reductions in genetic diversity and effective population size in *C. hystera* associated with the expected effects of selfing and loss of planktonic dispersal (Puritz et al., 2012). We estimated a surprisingly recent divergence time between the two species, about 6000 years or less, which implied a rapid rate of phenotypic evolution of life history traits including sex determination, spawning behavior, internal brooding of offspring, and live birth of juveniles.

151 *Patiria miniata* is a species of widely distributed asterinids (commonly called bat stars) that are
152 common in intertidal and shallow subtidal habitats from the temperate, open coasts of the northeastern
153 Pacific from southeastern Alaska to southern California (Kozloff, 1983). Adults are large (radius >5
154 cm), gonochoric broadcast spawners. Larvae are planktonic (like *C. pentagona*), but the eggs of *P.*
155 *miniata* are small and yolk-poor, and develop into long-lived feeding planktonic larval forms with
156 prolonged planktonic larval duration that includes substantial growth as well as development, followed
157 by settlement and metamorphosis into a benthic juvenile sea star (Strathmann, 1987). Those traits are
158 expected to facilitate long-distance dispersal and high rates of gene flow. We previously used a
159 combination of mitochondrial and nuclear markers to document large-scale population genetic
160 homogeneity over long distances separating some populations of *P. miniata*, including populations
161 from Vancouver Island and California (>1000 km) that are separated from each other by a large range
162 disjunction in Washington and Oregon where adults are rare or absent. By contrast, we discovered a
163 deep phylogeographic break in allele frequencies on a much smaller scale (<400 km) in British
164 Columbia between northern populations in Haida Gwaii and southern populations on Vancouver Island
165 separated from each other by Queen Charlotte Sound (Keever et al., 2009). Using targeted sampling of
166 those populations, and sequences from mitochondrial DNA plus six anonymous nuclear loci, we
167 estimated an old divergence time between populations, on the order of 280,000 years or more,
168 associated with a highly asymmetrical pattern of substantial gene flow (from north to south, but not in
169 the other direction) (McGovern et al., 2010). That pattern of gene flow was consistent with physical
170 models of larval dispersal in surface currents (Sunday et al., 2014), but was not sufficient to erase the
171 historical effects of a deep temporal split between northern and southern populations, which we
172 inferred to have been strongly influenced by environmental conditions associated with at least two
173 Pleistocene glaciation events. Molecular analyses of genes that encode gamete-recognition molecules
174 (Sunday & Hart, 2013) and laboratory mating experiments (Hart et al., 2014) showed evidence of

reproductive divergence between northern and southern populations caused by selection acting on gamete-binding proteins.

2.2 | RNA-seq data, assembly, and analysis

For both study systems we sampled a small number of individuals from two populations each, including one population of each *Cryptasterina* species, and a southern (Vancouver Island) and northern (Haida Gwaii) population of *P. miniata*. For *P. miniata* we analyzed data from ovary transcriptomes of three individuals for each population (total of six individuals, 12 gene copies per locus). We dissected gonad tissue samples, fixed them in RNAlater or Trizol, and transferred those samples to the BC Cancer Agency Genome Sciences Centre. For each sample, we collected short-read RNA-seq data using standard methods for library preparation and Illumina paired-end sequencing. The library development, sequencing methods, and RNA-seq data from *P. miniata* were previously described elsewhere (Hart, 2013; Hart & Foster, 2013). We previously assembled a small subset of reads from those transcriptomes for analysis in IM models of genes specifically involved in fertilization and possibly subject to selection associated with population divergence (Hart et al., 2014); here we analyze sequence variation in a much larger suite of loci from those transcriptomes.

For *Cryptasterina* spp., we analyzed data from ovary transcriptomes of three individuals of *C. pentagona* collected from an intertidal habitat at Kissing Point (19°13'S, 146°48'E) near Townsville on the coast of Queensland, plus data from four transcriptomes for the hermaphroditic gonad (ovary plus testis) of four individuals of *C. hystera* collected from shallow backreef coral rubble habitats on One Tree Island (23°30'S, 152°05'E) on the Great Barrier Reef (total of seven individuals, 14 gene copies per locus). The library development and sequencing methods for *Cryptasterina* spp. were the same as those we used for *P. miniata*. Raw sequence reads from those *Cryptasterina* spp. libraries were uploaded to the NCBI Sequence Read Archive (SRA) under BioProject PRJNA544828. We generated those data for use in an ongoing project to characterize and compare the gonad transcriptomes of those

two species specifically to discover coding sequences of genes that encode gamete-recognition molecules and analyze their divergence under selection in association with the life history and mating system differences between the two species. Here, we analyze a large suite of those genes from that transcriptome study using isolation-with-migration models.

Raw data preprocessing

In preparation for the assembly and mapping of sequence reads, we first trimmed and assessed the quality of the raw sequences. We downloaded raw reads from ovary RNA-seq libraries for *Patiria miniata* from the SRA database (BioProject PRJNA175319) using the sra toolkit (https://www.ncbi.nlm.nih.gov/sra/docs/toolkitsoft). Low-quality sequences and adapters were removed using the program Trimmomatic v. 0.32 (Bolger et al., 2014) and the Trimmomatic default settings of Trinity v. 2.6.5 (Grabherr et al., 2011). The overall quality of the Trimmomatic results were assessed with the program FastQC tools v. 0.11.3 (http://www.bioinformatics.babraham.ac.uk/projects/fastqc/).

Assembly and read mapping

There is no reference genome available for *Cryptasterina* spp., so a de novo reference transcriptome was created by assembling the cleaned reads from all libraries together using the default assembly parameters in Trinity v. 2.6.5 (Grabherr et al., 2011). We simplified that assembly by eliminating short alternative isoforms and retaining only the longest isoform for single genes using the perl program get_longest_isoform_seq_per_trinity_gene.pl in Trinity v 2.6.5 (Haas et al., 2013). For *P. miniata* we used the reference genome assembly Pmin_1.0 from the NCBI assembly database (BioProject PRJNA49323). We aligned each of the cleaned RNA-seq libraries from individual sea stars to the appropriate reference (the *Cryptasterina* spp. reference transcriptome or the *P. miniata* reference

genome) using the RNA-seq aligner STAR (Davis et al., 2013). Duplicate reads were marked with the Picard program MarkDuplicates (version 2.20.6, http://broadinstitute.github.io/picard).

Variant discovery

We followed the GATK best practices workflow for RNA-seq variant discovery of single nucleotide polymorphisms (SNPs) and indels (DePristo et al., 2011; McKenna et al., 2010) with some modifications. For each individual assembly the reads were hard clipped using the program SplitNCigarReads (version 4.1.2.0, https://gatk.broadinstitute.org/hc/en-us/articles/360036734471-SplitNCigarReads) to remove overhanging reads. We used HaplotypeCaller (version 4.1.2.0, https://gatk.broadinstitute.org/hc/en-us/articles/360036365812-HaplotypeCaller) to detect SNPs and indels using the default settings, including a minimum phred score of 20. We then filtered the results for variants using the program VariantFiltration (version 4.1.2.0, https://gatk.broadinstitute.org/hc/en-us/articles/360036733451-VariantFiltration). For *Cryptasterina* spp., we used the default filtering settings in the variant-calling perl program run_variant_calling.py in Trinity. For *Patiria miniata,* we used the following settings: quality depth < 2, StrandOddsRatio > 3, Fisher Strand > 30, RMSMappingQuality < 40. The variants were then incorporated into the reference using the program in the bcftools package called consensus (version 1.9, http://samtools.github.io/bcftools/bcftools.html).

Discovery of orthologous groups and gene alignment

We used the program OrthoFinder with the option for multiple sequence alignment (MSA) to find orthologous groups of genes across all assemblies from *Cryptasterina* spp. or across all assemblies from *Patiria miniata*. To reduce noise introduced by unidentified isoform variants, we modified the filters on the Orthofinder pairwise analysis to keep only a single gene from each assembly with a percentage length coverage of the protein hits of 90% or higher and an expectation score with a value e = 1×10^{-60} or lower. Orthogroups composed of single-copy genes from each of the seven individuals of

244 *Cryptasterina* spp. or each of the six individuals of *P. miniata* were retained for downstream analysis.
245 Each orthogroup was then populated with the variant data from each individual sea star. Gene copies in
246 each orthogroup were aligned using MUSCLE v. 3.8 with the default option for protein alignments
247 (Edgar et al., 2004). Gaps were removed from the *Cryptasterina* spp. data using PAL2NAL (Suyama et
248 al., 2006).

249 The Orthofinder filtration step resulted in 1941 orthogroups (or loci) from the *Cryptasterina*
250 gonad transcriptomes after applying that series of stringent quality-control filters for orthology and
251 sequence quality. Those filters were applied as part of our separate effort to characterize genes involved
252 in gamete recognition, but here we use those same transcriptome assemblies for demographic
253 inference. That stringent filtering (combined with our limited sampling of individuals within each
254 population or species) is expected to eliminate rare low-coverage polymorphisms from consideration
255 but is otherwise not expected to bias the observed pattern of nucleotide variation within or among loci
256 with respect to isolation-with-migration models and demographic inference. Because we assembled the
257 data from *Patiria miniata* to a reference genome (not a de novo transcriptome), and we collected very
258 large numbers of RNA-seq reads for the *P. miniata* study (see Hart & Foster, 2013), we had many more
259 possible loci available for analysis; to make the analyses of the two study systems approximately
260 comparable to each other, we limited our analysis of *P. miniata* to the first 1941 loci with alignment
261 lengths >300 bp.

262 That combined workflow using HaplotypeCaller, VariantFiltration, and consensus, followed by
263 Orthofinder to group genes into loci, resulted in a pair of gene copies for each diploid individual for
264 each of the 1941 loci in each study system. We treated these gene copies as haplotypes in isolation-
265 with-migration models, but we acknowledge that our sequence alignments may include some errors in
266 the workflow that resulted in incorrect phasing of polymorphisms into haplotypes. The challenges for
267 phasing polymorphisms in RNA-seq workflows for short-read data from non-model organisms without

a high-quality reference genome are well known and still not fully resolved (e.g., Krasileva et al., 2013; Louro et al., 2019; Wang et al., 2018). We are confident that our assemblies and sequence alignments represent as closely as possible the maternal and paternal genome copies in each individual sea star, and that IM models fitted to those data give high-quality insights into the demographic history of the populations from which those individuals were sampled, but we acknowledge that improvements in those assembly methods are needed.

2.3 | Isolation-with-migration model fitting

For each locus we noted the alignment length, and then grouped loci together into multilocus datasets for isolation-with-migration model fitting (the input files are given in the Supporting Information). We estimated demographic model parameters using IMa2p (Sethuraman & Hey, 2016) installed on the Compute Canada cluster called cedar. Because that installation was compiled to accept up to 1000 loci, for each study system we partitioned the 1941-locus dataset into two and analyzed them separately: one partition containing 999 loci from transcriptomes, and a second partition containing 942 loci from transcriptomes. To each of those datasets in each study system we added a mitochondrial DNA locus from our previous analyses for which a mutation rate calibration could be included in the input files. These are the same mtDNA sequence data in our previously published datasets, consisting of a combination of mitochondrial tRNAs, *cytochrome c oxidase subunit I* protein-coding sequences, and mitochondrial control region sequences (see McGovern et al. 2010; Puritz et al. 2012). We used the HKY substitution model in IMa2p for all loci, with an inheritance scalar of 0.25 for mtDNA and 1.0 for all genes from transcriptomes. We assumed a generation time (average age of breeding adults) of 3 years for smaller-bodied *Cryptasterina* spp. from the tropical and subtropical western Pacific, and 5 years for larger-bodied and slower-growing *Patiria miniata* from cooler temperate habitats in the northeastern Pacific.

Because we sampled just two populations for each study system, we fit a simple two-population model to the data, and we did not have to specify a population phylogeny or the rank order of population splitting times as in more complex multipopulation IMa2p models. Our simpler model has six demographic parameters including two historical parameters (population divergence time, *tau*; ancestral genetic diversity, *theta*), two genetic diversity estimates (*theta*, one for each sampled population), and two migration rates (immigration rates, *m*, into each population forward in time; in the model these are represented as migration rates from each population to the other backward in coalescent time).

A key difference from our previously published isolation-with-migration models is the use of a newer and more realistic mtDNA mutation rate calibration. Inclusion of a mutation rate calibration for one or more loci allows the estimates of model parameters (*tau*, *theta*) that are scaled by an unknown mutation rate to be converted to demographic parameters with ecologically relevant units, including the historical parameters for divergence time (t) and ancestral effective population size (N_{eA}) and effective size of each of the sampled populations (N_e). We previously used a very conservative (slow) rate calibration for echinoderm mtDNA based on an observed divergence rate of 4.5% between geminate pairs of sea urchin species separated from each other by the rise of the Isthmus of Panama about 3.1 million years ago (Lessios et al., 2001). More recent work suggests that mutation rates estimated from younger demographic or biogeographic calibration points tend to yield higher mutation rate estimates that are more likely to be close to true mutation rates (Hoareau, 2016). We used the estimate by Crandall et al. (2012) of the mtDNA mutation (not divergence) rate of 3.5% per million years for populations of a sea star (*Protoreaster nodosus*) associated with the demographic expansion of many benthic marine animal populations after the period of rapid sea level rise and flooding of the Sunda Shelf region approximately 14,500 years ago. This mutation rate calibration has the advantages that it is derived from a calibration point that is much closer in age to the temporal scale of late Pleiostocene

315 or Holocene population divergences in both of our study systems (in comparison to Pliocene
316 divergence between geminate species), and is derived from samples of mtDNA variation in a closely
317 related sea star (in comparison to mtDNA variation in distantly related sea urchins). A second key
318 improvement over our previously published analyses of isolation-with-migration models fitted to a
319 small number of loci from *Cryptasterina* species (Puritz et al., 2012) is our use of updated IMa2p
320 software that does not report incorrect estimates of relative mutation rates in the model output (see Hart
321 & Puritz, 2020).

322 The method in IMa2p uses Metropolis-coupled Markov chain Monte Carlo (MCMCMC)
323 optimization to search the space of genealogies and model parameter values and find the
324 neighbourhood of parameter values (the best-fit model) with the highest likelihood scores. After
325 finding that neighbourhood (via a burn-in period), the method then samples gene trees associated with
326 model fits from that stationary region of parameter space and reports a posterior distribution of
327 parameter value estimates based on those genealogies. Metropolis coupling allows the algorithm to
328 search broadly for improved parameter values that are different from a local optimum, by distributing
329 the optimization across multiple Markov chains using a heating scheme that forces heated chains to
330 search more broadly across the landscape of possible parameter values. That process can be
331 computationally slow, especially for large datasets with many loci for which many chains and heating
332 are needed for effective searching. That process can readily be accelerated in IMa2p by running
333 different chains on separate processors in parallel. For each of the study systems, we began with short
334 analyses (with few chains and small numbers of steps in the MCMCMC process) to find heating
335 schemes and prior distributions of demographic parameter values that seemed to lead to effective
336 searching of the parameter value space, and approximately captured the posterior distribution of
337 parameter values that had non-zero likelihoods. We also used those preliminary runs to estimate the
338 expected run time for more comprehensive searches with long burn-in periods and many chains (to find

339 the stationary part of the optimization process) and with large numbers of saved trees (to estimate
340 posterior distributions of parameter values). We then trimmed the prior distributions so that subsequent
341 runs focused only on the regions of parameter space with non-zero likelihoods across the prior range of
342 parameter values; this approach helped us to generate posterior distributions that densely sampled the
343 region of parameter space near the maximum likelihood estimate (MLE) of the parameter value, and
344 ignored other parts of the parameter value space with very low likelihoods.

345 For each data partition of each study system we then ran duplicate searches from different
346 random number seeds (different MCMCMC starting conditions; eight runs total; the individual output
347 files are given in Supporting Information, and include the command line string used to invoke the
348 MCMCMC search, the search parameters, and the priors on demographic parameter values). Each
349 search used 96 Markov chains each run in parallel on one of two nodes each with 48 processors (96
350 processors total; this is an efficient use of nodes and processors on cedar). We ran each search for a
351 burn-in period of $1x10^6$ steps in the Markov chain, followed by the same number of steps in the
352 stationary part of the distribution, during which we sampled the genealogy and parameter values at
353 intervals of 10 steps (for $1x10^5$ saved genealogies). IMa2p reports several quantities that can be used as
354 quality-control indicators (Roy 2020), including a plot of the trend in model likelihood scores over the
355 duration of the MCMCMC search and a plot of the trend in the estimate of the model divergence time
356 parameter *tau*, as well as comparisons of marginal estimates of model parameter values from the first
357 half of the set of sampled genealogies versus the second half of genealogies. We confirmed for each of
358 those eight runs that the model probability and the divergence time estimate lacked long-term trends in
359 the likelihood score (indicating that the search had achieved a stationary distribution without local
360 autocorrelation), and we confirmed close similarity between the two sets of model parameter estimates
361 (see Supporting Information). For each parameter in each study system, we show the four posterior
362 distributions as graphical summaries, which capture both the central tendency (the MLE) and the

uncertainty around it. Quantitative summaries of the results for all runs from both study systems are given in the appendices, including the value of the MLE for each parameter (the high point in the marginal posterior distribution) and the confidence limits around that mode (the upper and lower limits of the 95% highest posterior density or HPD).

Isolation-with-migration models like IMa2p use information from the shape of individual genealogies to infer demographic history. To illustrate example genealogies, we used TCS 1.21 (Clement, Posada, & Crandall, 2000) to infer and draw unrooted haplotype networks based on the statistical parsimony method.

3 | RESULTS

3.1 | *Cryptasterina* species

We analyzed data for 1941 loci from transcriptomes in which alignments varied from 12495 to 189 bp (mean 1769 bp). Because our input files were derived from reads mapped to a de novo transcriptome assembly in which the order of contigs was sorted by sequence length in the reference transcriptome, partitioning those alignments gave us two datasets that also differed in the range of lengths of the alignments: the first 999 loci ranged 12495–1404 bp; the last 942 loci ranged 1404–189 bp. In spite of those differences, we obtained similar demographic parameter value estimates from duplicate IMa2p analyses of the two partitions, and some of those results were closely similar to our previously published estimates of the history of divergence with gene flow in that study system. Those similarities suggest that our new data and transcriptome assemblies were not strongly affected by assembly errors (especially the sorting of SNPs into gene copies and haplotypes). The structure of haplotype networks inferred from several selected loci (Figure 1) that spanned that wide range of alignment lengths generally reflected the main features of those demographic parameter estimates, including low genetic diversity in *C. hystera*, and close relationships between *C. hystera* and some haplotypes from *C.*

pentagona, similar to the genealogies we observed in a small sample of loci in our previously published study (Puritz et al., 2012).

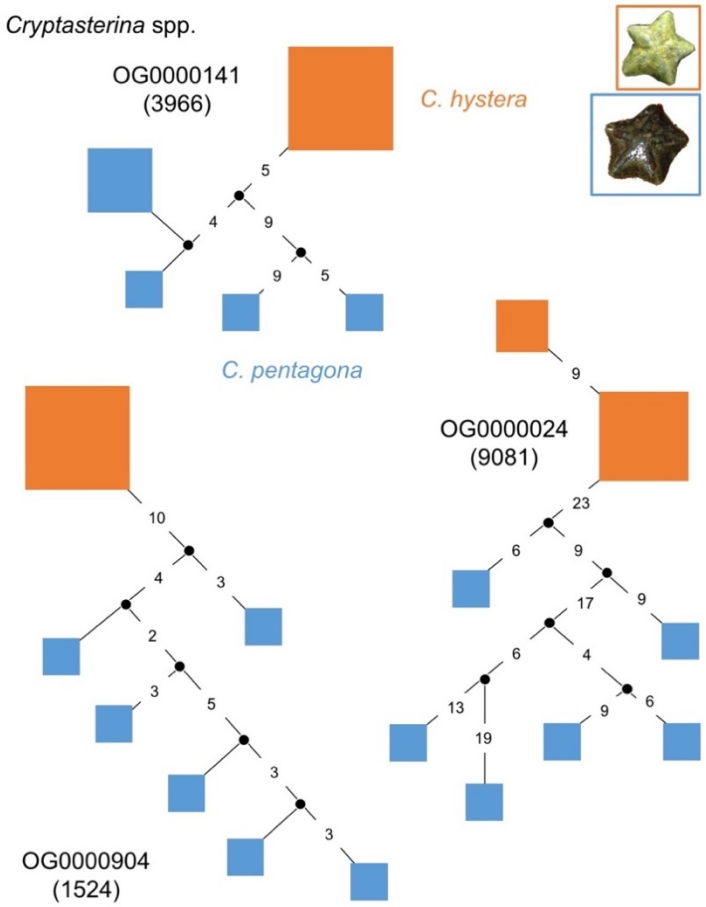

Figure 1 Three examples of gene genealogies that were analyzed in IMa2p models of divergence with gene flow between *Cryptasterina* spp. Gene names (and lengths of alignments) are contig names from the de novo transcriptome assembly. The alignment for each gene included six gene copies from one population sample of *C. pentagona* (blue), and eight gene copies from one population sample of *C. hystera* (orange). In each haplotype network the area of each symbol is proportional to its frequency in the alignment (from 1 to 8 occurrences in the total sample of 14 gene copies); black circles show nodes represented by unsampled haplotypes; numerals show the number of sequence differences between pairs of haplotypes when the value is greater than 1.

The most important similarity between our new analyses and our previously published results involved the population divergence time (t): our range of new MLEs (the high point of the four posterior distributions) was t~5700–8800 years, and that range included the point estimate of about 6000 years from our previously published study (Figure 2a). Our previous estimate was strongly affected by a software bug (since resolved) that greatly underestimated the age of the population divergence time; in our new results, the effect of resolving that bug was approximately counterbalanced by the effect of the discovery of much faster estimates of mtDNA mutation rate calibrations from more recent calibration events (in a more closely related taxon).

A second similarity involved estimates of effective population size, especially the large difference in N_e between *C. pentagona* (with separate sexes and outcrossing) and *C. hystera* (with selfing hermaphrodites). We estimated N_e~2000–3000 for *C. pentagona*, similar to our previously published estimate of N_e~3500 (Figure 3). Our estimate of N_e~5–10 for *C. hystera* was smaller than our previously published estimate (N_e~69), but several of our point estimates from transcriptomes fell within the very wide 95% HPD for our previously published estimate, and the qualitative nature of the species difference (much smaller N_e in *C. hystera* associated with its highly derived mating system) was not different from our previous analyses.

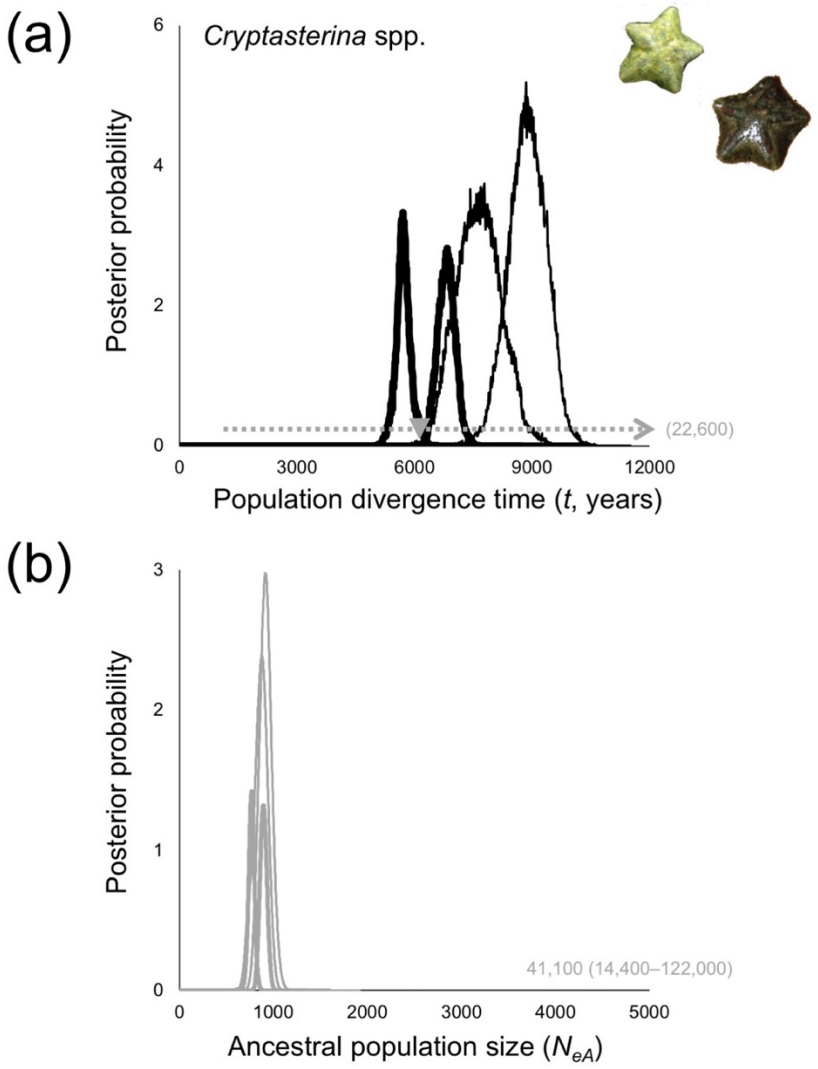

Figure 2 Posterior distributions of historical parameters from IMa2p models of divergence with gene flow between *Cryptasterina* species. In each plot the four curves show our new parameter value estimates based on duplicate analyses of datasets containing 999 loci from transcriptomes plus mtDNA (heavy lines) or 942 loci plus mtDNA (light lines). The high point of each curve indicates the maximum likelihood estimate (MLE) of the parameter value. The grey triangle shows the MLE from Puritz et al. (2012) based on few loci; the horizontal dotted line shows the 95% highest posterior density (HPD) estimate from our previous study; an arrow indicates a confidence interval from the previous estimate that was much wider than the priors (and the posteriors) in the new analyses in this study. Where the MLE or the HPD for the parameter values from Puritz et al. (2012) fell far outside the prior or the posterior distributions in this study, the previous estimate (and HPD) is shown in grey text. **(a)** Population divergence time (t). **(b)** Ancestral effective population size (N_{eA}).

That pattern of effective population size variation also illustrates a substantive difference from our previous study: the much greater precision and more narrow confidence limits around our estimates of all parameter values based on large numbers of loci from transcriptomes. It was common for us to find lower or upper HPD limits that fell within about 10% of the value of the MLE, in contrast to the very wide HPD limits associated with most parameter value estimates in our previous analysis based on few genes (e.g., Figure 3). One consequence of that greatly increased precision is apparent differences between MLEs from different data partitions and different replicate analyses. In particular, the limited overlap that we observed between the posterior distributions for some estimates of *t* for *Cryptasterina* species (Figure 2) suggests that those estimates were significantly different from each other, but those differences mainly reflect the narrow confidence limits around each estimate, and tend to exaggerate the apparent differences among replicates and partitions.

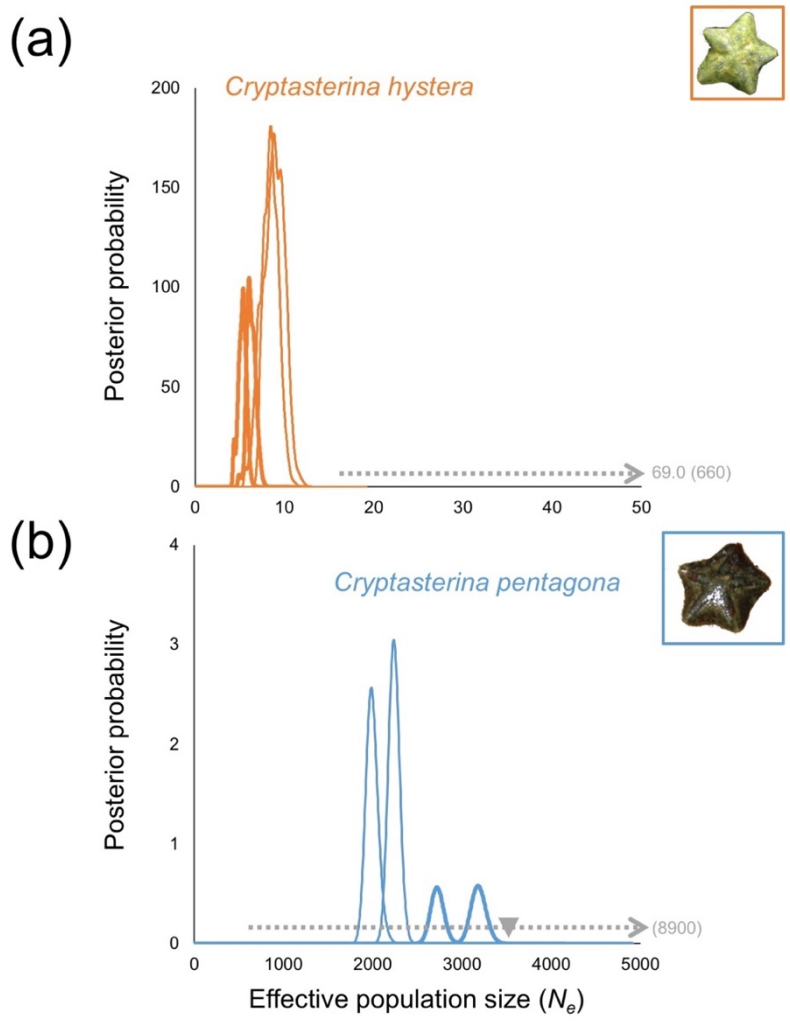

Figure 3 Posterior distributions of effective population size (N_e) from IMa2p models of divergence with gene flow between **(a)** *Cryptasterina hystera* (orange) and **(b)** *C. pentagona* (blue). In each plot the four curves show our new parameter value estimates based on duplicate analyses of datasets containing 999 loci from transcriptomes plus mtDNA (heavy lines) or 942 loci plus mtDNA (light lines). The high point of each curve indicates the maximum likelihood estimate (MLE) of the parameter value. The grey triangle shows the MLE from Puritz et al. (2012) based on few loci; the horizontal dotted line shows the 95% highest posterior density (HPD) estimate from our previous study; an arrow indicates a confidence interval from the previous estimate that was much wider than the priors (and the posteriors) in the new analyses in this study. Where the MLE or the HPD for the parameter values from Puritz et al. (2012) fell far outside the prior or the posterior distributions in this study, the previous estimate (and HPD) is shown in grey text.

A second notable difference from our previous results was much lower MLEs for the other historical parameter (ancestral effective population size; Figure 2), which ranged N_{eA}~700–900 and all fell far outside the wide confidence limits around our previous estimate. This difference seems to reflect real improvements in the coalescent information content of the new transcriptome data over our previous analyses of a small dataset of haplotypes from two nuclear introns, as well as the effects of an improved mutation rate calibration. Small datasets often contain too little information from old coalescent events to resolve both the population divergence time and the ancestral population size parameters in these models, and our new data seem to help in that resolution. The new MLEs also seem biologically realistic in the sense that they indicated similar orders of magnitude for the effective population size of the ancestral population (Figure 2b) and the descendant *C. pentagona* lineage (Figure 3b), which are assumed to both have the ancestral life history traits still found in *C. pentagona* populations (and in many other asterinid sea star species), in comparison to effective population size two orders of magnitude lower in *C. hystera* (Figure 3a). Together, our new estimates point to just one substantial change in effective population size (in *C. hystera*) that was associated with the evolution of selfing hermaphroditism, inbreeding, and expected loss of genetic diversity. By contrast, our previous analyses indicated a very large ancestral population size that was associated with two reductions in N_e in the descendant species: one modest reduction in N_e in *C. pentagona*, and a more severe reduction in N_e in *C. hystera*. Our new analyses suggest that conclusion was probably not correct.

The third notable difference from our previous results was the discovery of non-zero gene flow (m) during the history of divergence between *Cryptasterina* species. Our previous results indicated that immigration rates were not significantly different from zero in both directions (into *C. hystera*, and into *C. pentagona*) based on a likelihood ratio test of nested models with and without gene flow. The shapes of the posterior distributions for immigration from *C. pentagona* into *C. hystera* all clearly excluded m=0 (Figure 4a), but suggested that this immigration rate was very low, on the order of $2Nm$<0.01. By

contrast, the shapes of the posterior distributions for immigration into *C. pentagona* were similar to those from our previous analyses (with a MLE of m=0, and a fat tail of lower likelihoods for non-zero values of m; Figure 4b), and suggested that gene flow from *C. hystera* into *C. pentagona* was zero.

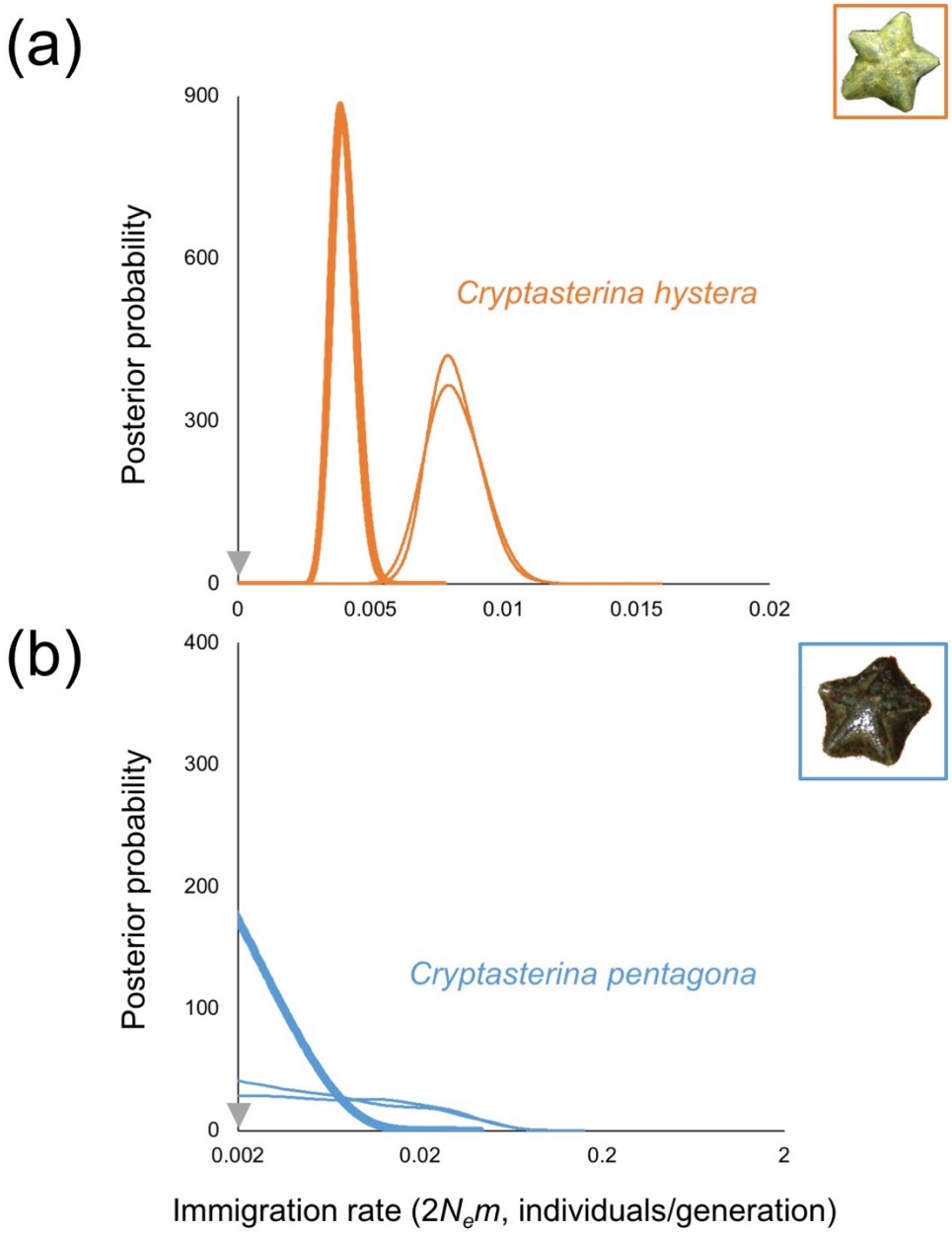

Figure 4 Posterior distributions of immigration rates ($2N_em$) from IMa2p models of divergence with gene flow into **(a)** *Cryptasterina hystera* (orange) and **(b)** *C. pentagona* (blue). In each plot the four curves show our new parameter value estimates based on duplicate analyses of datasets containing 999 loci from transcriptomes plus mtDNA (heavy lines) or 942 loci plus mtDNA (light lines). The high point of each curve indicates the maximum likelihood estimate (MLE) of the parameter value. The grey triangle shows the MLE from Puritz et al. (2012) based on few loci; no confidence interval is shown for gene flow from our previous study, where we estimated that both gene flow parameters were not significantly different from zero by a likelihood ratio test.

One interpretation of those posterior distributions is that a small amount of hybridization with *C. pentagona* (followed by selfing in the descendants) has occurred among some *C. hystera* lineages. That interpretation is consistent with the discovery that gametes of the two species are compatible in the lab, and that hybrid offspring from laboratory fertilizations are viable (M. Byrne, unpublished data).

An alternative interpretation is that extant *C. hystera* populations harbor ancestral polymorphisms at some loci that are also found among *C. pentagona*, and that the short time since the two species diverged has led to incomplete lineage sorting including some relatively recent mutations that arose in the ancestral *Cryptasterina* population but have been misidentified by the IMa2p algorithm as gene flow events (Cruickshank & Hahn, 2014; Hey et al., 2015). The small magnitude of the gene flow into *C. hystera* ($2Nm$<0.01, or fewer than one individual per hundred generations) was consistent with either of those interpretations. If these data do reflect hybridization with *C. pentagona*, the magnitude of the gene flow estimate suggested that this hybridization has probably not been ecologically important to the population biology of *C. hystera*.

3.2 | *Patiria miniata*

The 1941 loci we analyzed varied in length from 4997 to 302 bp (mean 2187 bp, similar to the mean length of alignments we analyzed from *Cryptasterina* spp.). Because our input files were derived from a reference-guided assembly organized by gene number in the reference genome (and not by contig length as in the *Cryptasterina* de novo assembly), the two partitioned datasets for *Patiria miniata* contained loci of similar lengths: 1992 bp (range 4997–313) for the partition containing 999 loci, and 2394 bp (range 4894–304) for the partition containing 942 loci. Examples of haplotype networks inferred from randomly selected loci showed considerable coalescent information (Figure 5), including differences between populations in the coalescent depth of haplotype differences (that represent differences in genetic diversity within samples), closely related haplotypes sampled in different populations (that might represent ancestral polymorphisms), and identical haplotypes sampled in individuals from different populations (that might represent gene flow events). Although the overall level of genetic variation was high, we often observed in the same genealogy one or more haplotypes represented by at least two identical gene copies from the same or from different individuals. That observation suggests that our workflow for sorting polymorphisms into haplotypes was not strongly

affected by large numbers of errors (because such errors should cause identical gene copies from libraries for different individual sea stars to instead differ from each other due to errors in haplotype calling in the workflow for analyzing each library).

In contrast to our new analyses of *Cryptasterina* spp, which confirmed our original estimate of the divergence time between them, our new analyses of *P. miniata* indicated a divergence time (t~70,000 years) for the phylogeographic break between northern and southern populations that was not as old as the divergence time in our previously published analyses (Figure 6a). The narrow confidence limits around the MLEs, and the close clustering of those MLEs, based on large samples of loci and a

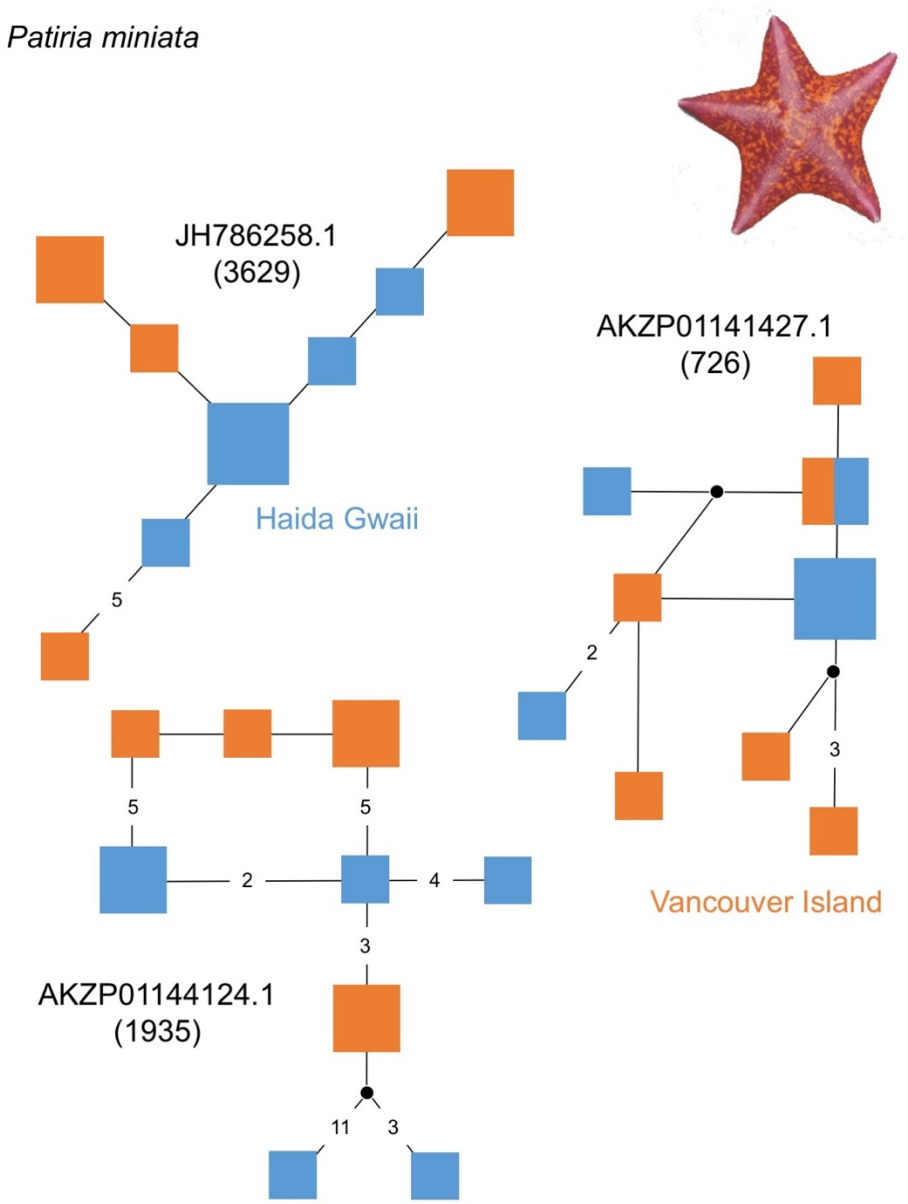

Figure 5 Three examples of gene genealogies that were analyzed in IMa2p models of divergence with gene flow between populations of *Patiria miniata*. Gene names (and lengths of alignments) are contig names from the Pmin_1.0 reference genome assembly. The alignment for each gene included six gene copies from a northern population sample on Haida Gwaii (blue), and six gene copies from a southern population sample on Vancouver Island (orange). In each haplotype network the area of each symbol is proportional to its frequency in the alignment (from 1 to 3 occurrences in the total sample of 12 gene copies); black circles show nodes represented by unsampled haplotypes; numerals show the number of sequence differences between pairs of haplotypes when the value is greater than 1.

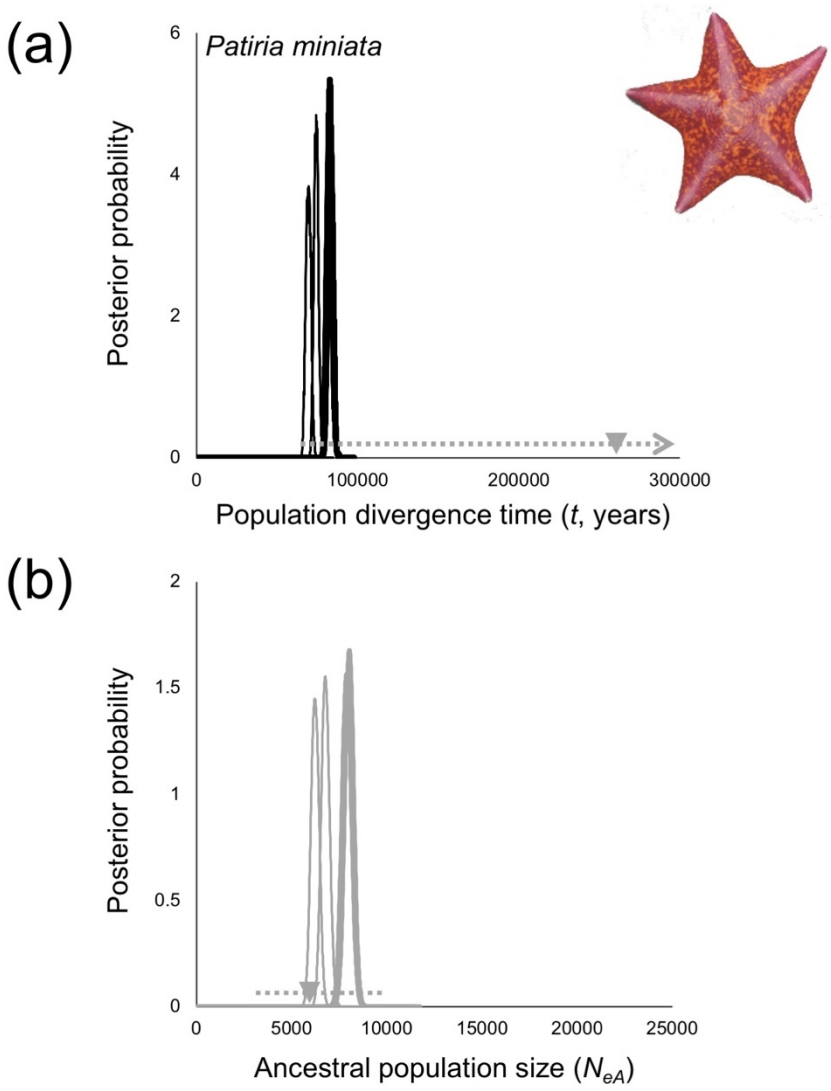

Figure 6 Posterior distributions of historical parameters from IMa2p models of divergence with gene flow between populations of *Patiria miniata*. In each plot the four curves show our new parameter value estimates based on duplicate analyses of datasets containing 999 loci from transcriptomes plus mtDNA (heavy lines) or 942 loci plus mtDNA (light lines). The high point of each curve indicates the maximum likelihood estimate (MLE) of the parameter value. The grey triangle shows the MLE from McGovern et al. (2010) based on few loci; the horizontal dotted line shows the 95% highest posterior density (HPD) estimate from our previous study; an arrow indicates a confidence interval from the previous estimate that was much wider than the priors (and the posteriors) in the new analyses in this study. Where the MLE or the HPD for the parameter values from McGovern et al. (2010) fell far outside the prior or the posterior distributions in this study, the previous estimate (and HPD) is shown in grey text. **(a)** Population divergence time (*t*). No value for the upper 95% HPD limit on divergence time is shown because in McGovern et al. (2010) we were not able to estimate an upper bound on the 95% HPD: the divergence time posterior was characterized by a mode at about 280,000 years, with a low but nonzero probability for much older divergence times that formed a long right-hand tail to the posterior and did not decline to zero. **(b)** Ancestral effective population size (N_{eA}). Note that in McGovern et al. (2010) we reported *theta* values (genetic diversity, not scaled for the mutation rate), not effective population sizes (scaled for the mutation rate). Here we show N_{eA} plotted on the same scale as our new estimates (relative to unscaled estimates of theta from our new data and analyses). For example, for the left-hand curve the MLE is N_{eA} ~6200 with *theta*~7.9; from McGovern et al. (2010) we estimated *theta*~7.0 (3.6-11.6), so on this scale the ancestral effective population size (and 95% HPD) in our previously published results was N_{eA}~5500 (2800-9100). Also note that in McGovern et al. (2010) we estimated that all three *theta* values in the model were not significantly different from each other by a likelihood ratio test.

more realistic mutation rate calibration, all suggest that these new estimates are more likely to reflect the history of divergence with gene flow across that phylogeographic break in bat stars.

553 Those new divergence time estimates are notable because they suggest that the origin of this
554 phylogeographic break coincided with the end of the previous warm interglacial period (called the
555 Sangamon period in North America) and the onset of the last (Wisconsinan) glaciation (Clague and
556 Ward 2011). Our previous estimate of that divergence time included a MLE of about 280,000 years,
557 but with a poorly resolved posterior distribution that included a broad right-hand tail of high
558 probabilities for much older divergence times, so our new estimates represent a considerable
559 improvement in precision as well as a likely improvement in accuracy. That new estimate also has a
560 simpler biogeographical interpretation associated with late-Pleistocene changes in climate and sea
561 level over just one glacial cycle (rather than two or more glacial cycles), and expected changes in the
562 distribution of marine populations and marine community composition caused by those extreme and
563 rapid environmental changes.

564 Like our analyses of *Cryptasterina* spp., these new analyses also show some of the ways in
565 which limited genomic sampling can prevent clear insights into historical demographic parameters,
566 and how expanded genomic sampling can overcome those limitations. Our previous analyses of the
567 phylogeographic break between populations of *P. miniata* included well-defined posterior distributions
568 for the ancestral effective population size in bat stars, but those small samples of few loci contained
569 too little coalescent information to resolve both ancestral effective population size and population
570 divergence time (like the corresponding constraint in our previous analysis of *Cryptasterina* spp.
571 where we successfully estimated t but failed to precisely estimate N_{eA}). Our new analyses gave
572 estimates of N_{eA}~6000-8000, similar to our previous estimates based on few loci, with new MLEs that
573 all fell within the confidence limits around our previous estimates (Figure 6b). The comparison
574 between the two study systems also shows that it may be difficult to predict which historical
575 demographic parameter – t in one case, N_{eA} in the other case – is likely to be incorrectly (or
576 imprecisely) estimated from small samples of loci.

Our new analyses gave effective population size estimates that were similar across replicates and data partitions (Figure 7), and with a broadly overlapping range of MLEs for the two populations (N_e~15,000-22,000). Those estimates are all greater than the range of MLEs for ancestral effective population size (Figure 6b) and suggest a history of modest population expansion (about two- to four-fold increase) on both sides of that phylogeographic break after the populations diverged during the last glaciation. By contrast, our previous analyses based on few loci suggested that recent and ancestral effective population sizes were not significantly different from each other (McGovern et al. 2010), and this now seems like an incorrect characterization of that specific aspect of bat star demographic history.

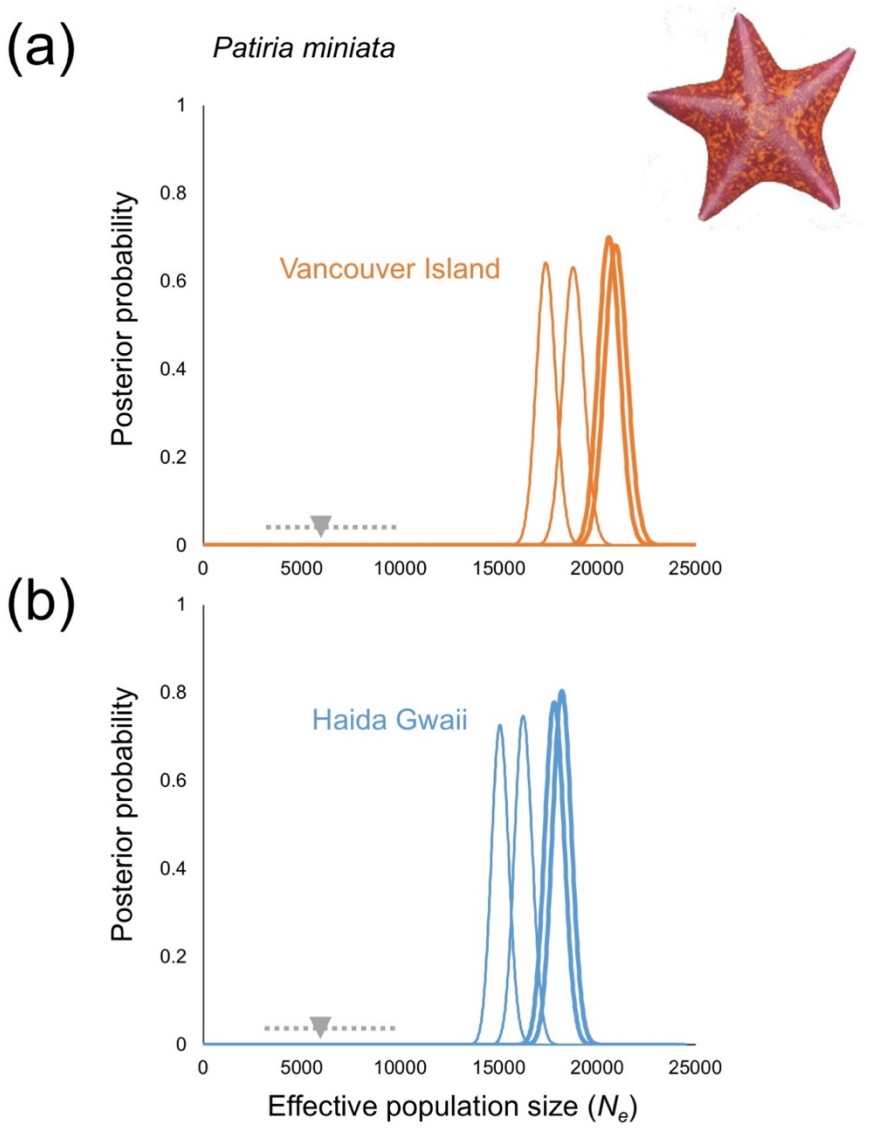

Figure 7 Posterior distributions of effective population size (N_e) from IMa2p models of divergence with gene flow between **(a)** Vancouver Island (orange) and **(b)** Haida Gwaii (blue) populations of *Patiria miniata*. In each plot the four curves show our new parameter value estimates based on duplicate analyses of datasets containing 999 loci from transcriptomes plus mtDNA (heavy lines) or 942 loci plus mtDNA (light lines). The high point of each curve indicates the maximum likelihood estimate (MLE) of the parameter value. The grey triangle shows the MLE from McGovern et al. (2010) based on few loci; the horizontal dotted line shows the 95% highest posterior density (HPD) estimate from our previous study.

Like our analyses of *Cryptasterina* spp., the most notable differences between our previous results and our new analyses are improvements in our characterization of gene flow. We previously reported asymmetrical gene flow, from Haida Gwaii to Vancouver Island (but not in the other direction), with ecologically significant rates of immigration into Vancouver Island ($2N_em$~10). Broad genomic sampling instead shows that gene flow between bat star populations separated by Queen Charlotte Sound is much more modest than we previously reported ($2N_em$~0.5; Figure 8), and approximately symmetrical between northern and southern populations. These new estimates point to

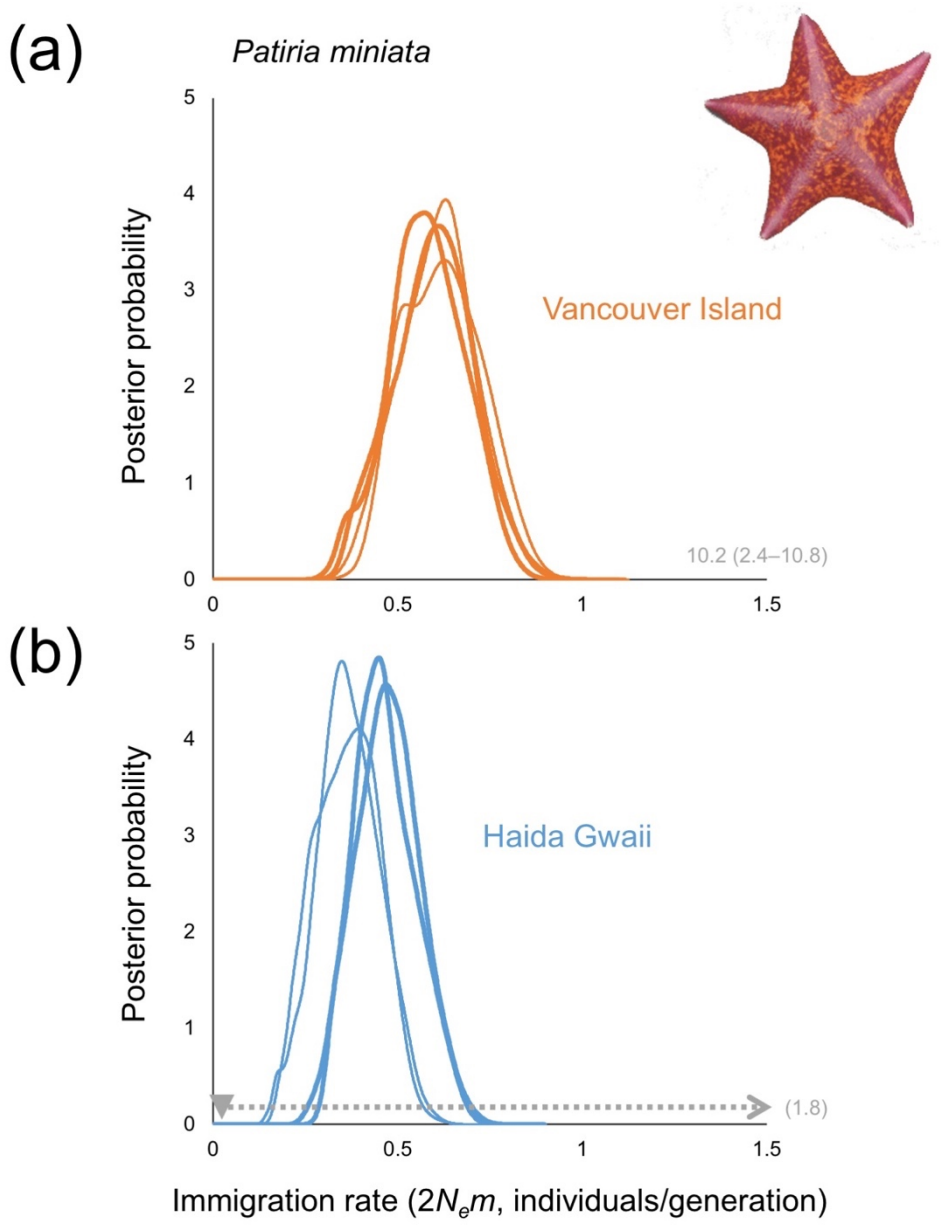

Figure 8 Posterior distributions of immigration rates ($2N_em$) from IMa2p models of divergence with gene flow into **(a)** Vancouver Island (orange) and **(b)** Haida Gwaii (blue). In each plot the four curves show our new parameter value estimates based on duplicate analyses of datasets containing 999 loci from transcriptomes plus mtDNA (heavy lines) or 942 loci plus mtDNA (light lines). The high point of each curve indicates the maximum likelihood estimate (MLE) of the parameter value. The grey triangle shows the MLE from McGovern et al. (2010) based on few loci; the horizontal dotted line shows the 95% highest posterior density (HPD) estimate from our previous study; an arrow indicates a confidence interval from the previous estimate that was much wider than the priors (and the posteriors) in the new analyses in this study. Where the MLE or the HPD for the parameter values from McGovern et al. (2010) fell far outside the prior or the posterior distributions in this study, the previous estimate (and HPD) is shown in grey text.

considerably stronger ecological and demographic isolation between northern and southern populations than we previously estimated, and those improved estimates help to make sense of other analyses that showed evidence for reproductive divergence in gamete compatibility and in genes that encode gamete-binding molecules (Sunday & Hart, 2013; Hart et al., 2014). Our new results suggest that reproductive divergence between bat star populations has evolved in the face of only modest ongoing immigration rates, rather than in the face of massive influx of northern individuals and alleles into southern populations as we previously reported.

4 | DISCUSSION

In our new study, we attempted to replicate and augment the headline results from two of our previous phylogeographic analyses of asterinid sea stars: old Pleiostocene divergence between populations of *Patiria miniata*, and recent Holocene divergence between species of *Crypasterina*. Such replication studies are needed but uncommon in evolutionary ecology (Nakagawa & Parker, 2015). A significant obstacle to replication is the perception that replicated results are not novel or interesting (Forstmeier et al., 2017), but our replication led to both better resolution of some parameter values and more realistic values for others, and a better understanding of the population biology of both study systems. Our approach here used much more data (but not qualitatively different data), and an updated version of the same IM analytical method (rather than a qualitatively different method, such as approximate Bayesian computation; Beaumont, 2010), for samples from the same biological populations in both study systems. That approach fulfills the definition of a partial replication (i.e., a "fairly narrowly defined biological phenomenon mostly limited to a population, strain, or locality"; Nakagawa & Parker, 2015).

Our replication study shows that some of our previous discoveries were replicated, including Holocene divergence time with very little gene flow between *Cryptasterina* species, and Pleistocene divergence between northern and southern populations across the major phylogeographic break in

638 *Patiria miniata*. We interpret the similarities, especially the broadly similar estimates of recent
639 divergence between *Cryptasterina* species (associated with the evolution of derived mating system
640 traits in *C. hystera*), and much older divergence between populations of *P. miniata* (associated with the
641 last glaciation event in North America), as confirmation of our previous discoveries.

642 By contrast, other previously reported features of divergence-with-gene-flow in these two study
643 systems were not replicated or were only partially replicated in our new analyses, including the pattern
644 of historical changes in effective population sizes in *Cryptasterina* species and the symmetry and
645 magnitude of gene flow between populations of *P. miniata*. In our new analyses, reduced population
646 size in *Cryptasterina* was limited to *C. hystera*; and gene flow in *P. miniata* was an order of magnitude
647 lower than we previously reported, and symmetrical across the phylogeographic break. Updating our
648 mutation rate calibrations also greatly improved the accuracy of those historical parameter value
649 estimates and led to more realistic estimates of effective population sizes after population divergence
650 (or after speciation).

651 Why does broader genomic sampling lead to improved precision? We interpret those
652 improvements as mainly consequences of greatly increased coalescent information content in hundreds
653 of loci compared to ≤7 loci in our previous "unplugged" studies. This effect is well-known in IM
654 model-fitting, and is most commonly identified as unresolved right-hand tails in posterior distributions
655 that have high non-zero probabilities associated with a broad range of high parameter values.
656 Unfortunately, this problem can be hard to identify in any given result. In our previous studies based on
657 few loci we obtained poorly resolved posterior distributions for some historical parameters (e.g.,
658 divergence time between *P. miniata* populations, ancestral population size in *Cryptasterina*) that were
659 readily flagged as possibly imprecise and therefore possibly not accurate as well (McGovern et al.
660 2010). But in those earlier studies we also obtained seemingly well-resolved posterior distributions for
661 some other parameter values (gene flow in both study systems) that we could not foresee would turn

662 out to be incorrect except by attempting to replicate the study with much more data (McGovern et al.,
663 2010; Puritz et al., 2012). We interpret differences like this as a consequence of stochastic differences
664 between the shape and coalescent depth of a small sample of gene trees from few loci in comparison to
665 the true population history of the organisms and the average shape and coalescent depth of gene trees
666 across the genome.

667 Are such mixed results (replicating some discoveries, and rejecting or modifying other
668 conclusions) common for replication studies? Kelly (2019) found that few (0.023%) studies in
669 evolutionary ecology were characterized as replications by the authors, so the relative frequencies of
670 successful or partial or failed replications is not known. A much longer history of replication attempts
671 will be needed to know whether our results are typical, and whether the addition of data from RNA-seq
672 (or other genome-wide sampling methods) and updates of mutation rate calibrations will often lead to
673 substantially different conclusions about isolation with gene flow.

674 Phylogeographic studies of benthic marine animals provide a rich source of previous
675 discoveries based on few loci that might reward replication efforts using genome-wide sampling in IM
676 models. But where should these excellent and expensive tools be applied? Phylogeographic surveys of
677 population differentiation based on mtDNA or small samples of other loci will probably often point
678 directly to the specific parts of such systems that are likely to reward broad genomic sampling of many
679 loci from few individuals. In the case of our analyses of the phylogeographic break in *Patiria miniata*,
680 we would not have originally focused on populations from British Columbia for studies of gamete-
681 recognition genes (Sunday and Hart, 2013), gamete compatibility (Hart et al. 2014), or genome-wide
682 genetic divergence (this study), if we had not first carried out a survey across the geographic range of
683 the species and identified that strong, deep phylogeographic break between British Columbian
684 populations. In an example similar to our studies of *Cryptasterina* species, Florin & Hoglund (2008)
685 documented strong genetic differentiation at a small number of loci in co-occurring flounder

686 (*Platichthys flesus*) populations with different life history and spawning behaviours in the Baltic Sea.
687 Using genome-wide sampling of SNP variation in an isolation-with-gene-flow framework, Momigliano
688 et al. (2018) then showed that these ecotypes probably represent cryptic species that diverged only a
689 few thousand generations ago. We suspect that many other previous range-wide phylogeographic
690 surveys that used microsatellites or mtDNA might often point toward specific parts of other study
691 systems that would reward the judicious application of RNA-seq or other methods to unpack the
692 genome-wide temporal patterns of genetic divergence with gene flow associated with specific aspects
693 of population structure or phenotypic divergence, as proposed by Bowen et al. (2014) at the close of the
694 "unplugged" era.

695 **5 | CONCLUSIONS**

696 Our study using genome-wide sampling of transcriptomes successfully replicated some previous results
697 (especially the relative ages of population divergence and speciation events) based on few loci but
698 failed to replicate others (especially our previous characterizations of gene flow). We identified
699 important improvements in phylogeographic understanding relative to " unplugged" results based on
700 amplicon sequencing of few loci. Improved precision for all parameter estimates, greater accuracy
701 (associated with better precision and with more realistic mutation rate calibrations), and increased
702 biological realism all followed from our better datasets.

703 Our comparative analyses of these two study systems are a source of both satisfaction and
704 additional interest because they suggest that many previous phylogeographic studies could include a
705 mix of both more and less reliable conclusions based on few loci. The need to add loci is widely
706 acknowledged by both theoreticians and empiricists (Edwards & Beerlie, 2000; Felsenstein, 2006;
707 Pinho & Hey, 2010; Wang & Hey, 2010), and genomic methods have been widely adopted in new IM
708 studies (Andrew, Kane, Baute, Grassa, & Rieseberg, 2013; Leache, Harris, Maliska, & Linkem, 2013;
709 McCormack et al., 2013; Morales, Jackson, Dewey, O'Meara, & Carstens, 2017; Oswald, Overcast,

Mauck, Andersen, & Smith, 2017). However, there has not been a concerted effort to reconsider previously published characterizations of isolation with migration based on few loci. The improvements we observed here argue for additional replication studies using high-throughput sequencing applied to carefully chosen contexts or populations in other areas of marine phylogeography that were previously analyzed using "unplugged" approaches. The improved understanding of population divergence and speciation in the sea that could be generated using these methods is important for developing informed biodiversity management and conservation strategies, and may be especially important as global ocean change is rapidly altering the persistence and dynamics of many marine species and populations.

ACKNOWLEDGEMENTS

Thanks to Jason Addison, Rick Grosberg, Carson Keever, Christine Konrad, Kevin Learning, Peter Marko, Tammy McGovern, Iva Popovic, Jenn Sunday, and Rob Toonen for previous contributions to sampling and analyses of our earlier published studies of isolation-with-migration in these sea stars, and to Demian Koop for help with collection of tissue samples.

REFERENCES

Andrew, R. L., Kane, N. C., Baute, G. J., Grassa, C. J., & Rieseberg, L. H. (2013). Recent nonhybrid origin of sunflower ecotypes in a novel habitat. *Molecular Ecology, 22,* 799–813. doi:10.1111/mec.12038

Barbosa, S. S., Klanten, S. O., Puritz J. B., Toonen, R. J., & Byrne, M. (2013. Very fine-scale population genetic structure of sympatric asterinid sea stars with benthic and pelagic larvae: influence of mating system and dispersal potential. *Biological Journal of the Linnean Society, 108,* 821–833. doi:10.1111/bij.12006

Beaumont, M. A. (2010). Approximate Bayesian computation in evolution and ecology. *Annual Review of Ecology, Evolution, and Systematics. 41.* 379–406. doi:10.1146/annurev-ecolsys-102209-144621

Bolger, A. M., Lohse, M., & Usadel, B. (2014). Trimmomatic: a flexible trimmer for Illumina sequence data. *Bioinformatics*, *30*, 2114–2120. doi:10.1093/bioinformatics/btu170

Bowen, B. W., Shanker, K., Yasuda, N., Celia, M., Malay, M. C., von der Heyden, S., … Toonen, R. J. (2014). Phylogeography unplugged: comparative surveys in the genomic era. *Bulletin of Marine Science, 90,* 13–46. doi:10.5343/bms.2013.1007

Byrne, M. (2005). Viviparity in the sea star *Cryptasterina hystera* (Asterinidae)—conserved and modified features in reproduction and development. *Biological Bulletin*, *208*, 81–91. doi:10.2307/3593116

Byrne, M. (2006). Life history diversity and evolution in the Asterinidae. *Integrative and Comparative Biology, 46*, 243–254. doi:10.1093/icb/icj033

Byrne, M., Hart, M. W., Cerra, A., & Cisternas, P. (2003). Reproduction and larval morphology of broadcasting and viviparous species in the *Cryptasterina* species complex. *Biological Bulletin, 205*, 285–294. doi:10.2307/1543292

Cahais, V., Gayral, P., Tsagkogeorga, G., Melo-Ferreira, J., Ballenghien, M., Weinert, L., … Galtier, N. (2012). Reference-free transcriptome assembly in non-model animals from next-generation sequencing data. *Molecular Ecology Resources, 12,* 834–845. doi:10.1111/j.1755-0998.2012.03148.x

Clement, M., Posada, D., & Crandall, K. A. (2000). TCS : a computer program to estimate gene genealogies. *Molecular Ecology, 9,* 1657–1659. doi:10.1046/j.1365-294x.2000.01020.x

Crandall, E. D., Sbrocco, E. J., DeBoer, T. S., Barber, P. H., & Carpenter, K. E. (2012). Expansion dating: Calibrating molecular clocks in marine species from expansions onto the Sunda Shelf following the last glacial maximum. *Molecular Biology and Evolution, 29,* 707–719. doi: 10.1111/mec.12796

Cruickshank, T. E., & Hahn, M. W. (2014) Reanalysis suggests that genomic islands of speciation are due to reduced diversity, not reduced gene flow. *Molecular Ecology, 23,* 3133-3157. doi:10.1111/mec.12796

Dartnall, A. J., Byrne, M., Collins, J., & Hart, M.W. (2003). A new viviparous species of asterinid (Echinodermata, Asteroidea, Asterinidae) and a new genus to accommodate the species of pan-tropical exiguoid sea stars. *Zootaxa, 359*, 1–14. doi:10.11646/zootaxa.359.1.1

764 Davey, J. W., Hohenlohe, P. A., Etter, P. D., Boone, J. Q., Catchen, J. M., & Blaxter, M. L. (2011).
765 Genome-wide genetic marker discovery and genotyping using next-generation sequencing. *Nature*
766 *Reviews Genetics, 12,* 499–510. doi:10.1038/nrg3012

767 DePristo, M. A., Banks, E., Poplin, R., Garimella, K. V., Maguire, J. R., Hartl, C., … Daly, M. J.
768 (2011). A framework for variation discovery and genotyping using next-generation DNA
769 sequencing data. *Nature Genetics*, 43, 491–498. doi:10.1038/ng.806

770 Dobin, A., Davis, C. A., Schlesinger, F., Drenkow, J., Zaleski, C., Jha, S., … Gingeras, T. R. (2013).
771 STAR: ultrafast universal RNA-seq aligner. *Bioinformatics, 29,* 15–21.
772 doi:10.1093/bioinformatics/bts635

773 Edgar, R. C. (2004). MUSCLE: multiple sequence alignment with high accuracy and high throughput.
774 *Nucleic Acids Research*, *32*, 1792–1797. doi:10.1093/nar/gkh340

775 Edwards, S. V., & Beerli, P. (2000). Gene divergence, population divergence, and the variance in
776 coalescence time in phylogeographic studies. *Evolution, 54,* 1839–1954. doi:10.1111/j.0014-
777 3820.2000.tb01231.x

778 Felsenstein, J. (2006). Accuracy of coalescent likelihood estimates: Do we need more sites, more
779 sequences, or more loci? *Molecular Biology and Evolution, 23,* 691–700.
780 doi:10.1093/molbev/msj079

781 Florin, A. B., & Hoglund J. (2008). Population structure of flounder (*Platichthys flesus*) in the Baltic
782 Sea: differences among demersal and pelagic spawners. *Heredity, 101,* 27–38.
783 doi:10.1038/hdy.2008.22

784 Forstmeier, W., Wagenmakers, E.-J., & Parker, T. H. (2017). Detecting and avoiding likely false-
785 positive findings – a practical guide. *Biological Reviews, 92,* 1941–1968. doi:10.1111/brv.12315

786 Grabherr, M. G., Haas, B. J., Yassour, M., Levin, J. Z., Thompson, D. A., Amit, I., … Regev, V.
787 (2011). Full-length transcriptome assembly from RNA-Seq data without a reference genome. *Nature*
788 *Biotechnology, 29*, 644–652. doi:10.1038/nbt.1883

789 Haas, B. J., Papanicolaou, A., Yassour, M., Grabherr, M., Blood, P. D., Bowden, J., … Regev, A.
790 (2013). De novo transcript sequence reconstruction from RNA-seq using the Trinity platform for
791 reference generation and analysis. *Nature Protocols, 8*, 494–512. doi:10.1038/nprot.2013.084

792 Hart, M. W. (2013). Structure and evolution of the sea star egg receptor for sperm bindin. *Molecular*
793 *Ecology, 22*, 2143–2156. doi:10.1111/mec.12251

794 Hart, M. W., & Foster, A. (2013). Highly expressed genes in gonads of the bat star *Patiria miniata*:
795 gene ontology, expression differences, and gamete recognition loci. *Invertebrate Biology, 132*, 241–
796 250. doi: 10.1111/ivb.12029

797 Hart, M. W., & Marko, P. B. (2010). It's about time: divergence, demography, and the evolution of
798 developmental modes in marine invertebrates. *Integrative and Comparative Biology, 50*, 643–661.
799 doi:10.1093/icb/icq068

800 Hart, M. W., & Puritz, J. B.. (2020). Correction to 'Extraordinarily rapid life history divergence
801 between *Cryptasterina* sea star species'. *Proceedings of the Royal Society B, 287*, 20201325.
802 doi:10.1098/rspb.2020.1325

803 Hart, M. W., Byrne, M., & Smith M. J. (1997). Molecular phylogenetic analysis of life-history
804 evolution in asterinid starfish. *Evolution, 51,* 1848–1861. doi:10.2307/2411007

805 Hart, M. W., Sunday, J. M., Popovic, I., Learning, K. J., & Konrad, C. M. (2014). Incipient speciation
806 of sea star populations by adaptive gamete recognition coevolution. *Evolution, 68,* 1294–1305. doi:
807 10.1111/evo.12352

808 Hey, J. (2010a). Isolation with migration models for more than two populations. *Molecular Biology*
809 *and Evolution, 27,* 905–920. doi:10.1093/molbev/msp296

810 Hey, J. (2010b). The divergence of chimpanzee species and subspecies as revealed in multipopulation
811 isolation-with-migration analyses. *Molecular Biology and Evolution, 27,* 921–933.
812 doi:10.1093/molbev/msp298

813 Hey, J., & Nielsen, R. (2004). Multilocus methods for estimating population sizes, migration rates and
814 divergence time, with applications to the divergence of *Drosophila pseudoobscura* and *D.*
815 *persimilis. Genetics, 167*, 747–760. doi:10.1534/genetics.103.024182

816 Hey, J., Chung, Y. J., & Sethuraman, A. (2015). On the occurrence of false positives in tests of
817 migration under an isolation-with-migration model. *Molecular Ecology, 24,* 5078–5083.
818 doi:10.1111/mec.13381

819 Hey, J., Chung, Y. J., Sethuraman, A., Lachance, J., Tishkoff, S., Sousa, V. C., & Wang, Y. (2018).
820 Phylogeny estimation by integration over isolation with migration models. *Molecular Biology and*
821 *Evolution, 35,* 2805–2818. doi:10.1093/molbev/msy162

822 Hoareau, T. B. (2016). Late glacial demographic expansion motivates a clock overhaul for population
823 genetics. *Systematic Biology, 65,* 449–464. doi:10.1093/sysbio/syv120

824 Keever, C. C., Puritz, J. B., Addison, J. A., Byrne, M., Grosberg, R. K., Toonen, R. J., & Hart, M. W.
825 (2013). Shallow gene pools in the high intertidal: extreme loss of genetic diversity in viviparous sea
826 stars (*Parvulastra*). *Biology Letters, 9,* 20130551. doi:10.1098/rsbl.2013.0551

827 Keever, C. C., Sunday, J., Puritz, J. B., Addison, J. A., Toonen, R. J., Grosberg, R. K., & Hart, M. W.
828 (2009). Discordant distribution of populations and genetic variation in a sea star with high dispersal
829 potential. *Evolution, 63,* 3214–3227. doi:10.1111/j.1558-5646.2009.00801.x

830 Kelly, C. D. (2019). Rate and success of study replication in ecology and evolution. *PeerJ, 7,* e7654.
831 doi:10.7717/peerj.7654

832 Kozloff, E. N. (1983). *Seashore life of the northern Pacific coast.* Seattle, WA: University of
833 Washington Press.

834 Krasileva, D. J., Buffalo, V., Bailey, P., Pearce, S., Ayling, S., Tabbita, F.,…Dubcovsky, J. (2013).
835 Separating homeologs by phasing in the tetraploid wheat transcriptome. *Genome Biology, 14,* R66.
836 doi:10.1186/gb-2013-14-6-r66

837 Leache, A. D., Harris, R. B., Maliska, M. E., & Linkem, C. W. (2013). Comparative species divergence
838 across eight triplets of spiny lizards (*Sceloporus*) using genomic sequence data. *Genome Biology*
839 *and Evolution, 5,* 2410–2419. doi:10.1093/gbe/evt186

840 Lessios, H. A., Kessing, B. D. & Pearse, J. S. (2001). Population structure and speciation in tropical
841 seas: global phylogeography of the sea urchin *Diadema*. *Evolution, 55,* 955–975.
842 doi:10.1111/j.0014-3820.2001.tb00613.x

843 Louro, B., De Moro, G., Garcia, C., Cox, C. J., Verissimo, A., Sabatino, S. J.,…Canario, A. V. M.
844 (2019). A haplotype-resolved draft genome of the European sardine (*Sardina pilchardus*).
845 *Gigascience, 8*, giz059. doi:10.1093/gigascience/giz059

846 McCormack, J. E., Hird, S. M., Zellmer, A. J., Carstens, B. C., & Brumfield, R. T. (2013). Applications
847 of next-generation sequencing to phylogeography and phylogenetics. *Molecular Phylogenetics and*
848 *Evolution, 66,* 526–538. doi:10.1016/j.ympev.2011.12.007

849 McGovern, T. M., Keever, C. C., Saski, C. A., Hart, M. W., & Marko, P. B. (2010). Divergence
850 genetics analysis reveals historical population genetic processes leading to contrasting
851 phylogeographic patterns in co-distributed species. *Molecular Ecology*, *19*, 5043–5060.
852 doi:10.1111/j.1365-294X.2010.04854.x

853 McKenna, A., Hanna, M., Banks, E., Sivachenko, A., Cibulskis, K., Kernytsky, A., … DePristo MA.
854 (2010). The Genome Analysis Toolkit: a MapReduce framework for analyzing next-generation
855 DNA sequencing data. *Genome Research, 20*, 1297-1303. doi:10.1101/gr.107524.110

856 Momigliano, P., Jokinen, H., Fraimout, A., Florin, A. B., Norkko, A., & Meriläa, J. (2018).
857 Extraordinarily rapid speciation in a marine fish. *Proceedings of the National Academy of Sciences*
858 *of the USA, 114,* 6074–6079. doi:10.1073/pnas.1615109114

859 Morales, A. E., Jackson, N. D., Dewey, T. A., O'Meara, B. C., & Carstens, B. C. (2017). Speciation
860 with gene flow in North American *Myotis* bats. *Systematic Biology, 66,* 440–452.
861 doi:10.1093/sysbio/syw100

862 Nadachowska-Brzyska, K., Burri, R., Olason, P. I., Kawakami, T., Smeds, L., & Ellegren, H. (2013).
863 Demographic divergence history of pied flycatcher and collared flycatcher inferred from whole-
864 genome resequencing data. *PLoS Genetics, 9,* 31003942. doi:10.1371/journal.pgen.1003942

865 Nakagawa, S., & Parker, T. H. (2015). Replicating research in ecology and evolution: feasibility,
866 incentives, and the cost-benefit conundrum. *BMC Biology, 13,* 88. doi:10.1186/s12915-015-0196-3

867 Oswald, J. A., Overcast, I., Mauck, W. M., Andersen, M. J., & Smith, B. T. (2017). Isolation with
868 asymmetric gene flow during the nonsynchronous divergence of dry forest birds. *Molecular Ecology,*
869 *26,* 1386–1400. doi:10.1111/mec.14013

870 Peterson, B. K., Weber, J. N., Kay, E. H., Fisher, H. S., & Hoekstra, H. E. (2012). Double digest
871 RADseq: an inexpensive method for de novo SNP discovery and genotyping in model and non-
872 model species. *PLoS ONE, 7*, e37135. doi:10.1371/journal.pone.0037135

873 Pinho, C., & Hey, J. (2010). Divergence with gene flow: models and data. *Annual Review of Ecology,*
874 *Evolution, and Systematics, 41,* 215–230. doi:10.1146/annurev-ecolsys-102209-144644

875 Puritz, J. B., & Lotterhos, K. E. (2018). Expressed exome capture sequencing: a method for cost-
876 effective exome sequencing for all organisms. *Molecular Ecology Resources, 18,* 1209–1222.
877 doi:10.1111/1755-0998.12905

878 Puritz, J. B., Keever, C. C., Addison, J. A., Barbosa, S. S., Byrne, M., Hart, M. W., … Toonen, R. J.
879 (2017). Life-history predicts past and present population connectivity in two sympatric sea stars.
880 *Ecology and Evolution, 7,* 3916–3930. doi:10.1002/ece3.2938

881 Puritz, J. B., Keever, C. C., Addison, J. A., Byrne, M., Hart, M. W., Grosberg, R. K., and Toonen, R. J.
882 (2012). Extraordinarily rapid life-history divergence in *Cryptasterina* sea star species. *Proceedings*
883 *of the Royal Society B,* 279, 3914–3922. doi:10.1098/rspb.2012.1343

884 Roy, V. (2020). Convergence diagnostics for Markov chain Monte Carlo. *Annual Review of Statistics*
885 *and its Application, 7*, 387–412. doi:10.1146/annurev-statistics-031219-041300

886 Selkoe, K. A., D'Aloia, C. C., Crandall, E. D., Iacchei, M., Liggins, L., Puritz, J. B.,…Toonen, R. J.
887 2016. A decade of seascape genetics: contributions to basic and applied marine connectivity. *Marine*
888 *Ecology Progress Series, 554,* 1–19. doi:10.3354/meps11792

889 Sethuraman, A., & Hey, J. (2016). IMa2p-parallel MCMC and inference of ancient demography under
890 the isolation with migration (IM) model. *Molecular Ecology Resources, 16,* 206–215.
891 doi:10.1111/1755-0998.12437

892 Strathmann, M. F. (1987). *Reproduction and development of marine invertebrates of the northern*
893 *Pacific coast.* Seattle, WA: University of Washington Press.

894 Sunday, J. M., & Hart, M. W. (2013). Sea star populations diverge by positive selection at a sperm-egg
895 compatibility locus. *Ecology and Evolution, 3,* 640–654. doi:10.1002/ece3.487

896 Sunday, J. M., Palen, W., Foreman, M., Popovic, I., & Hart, M. W. (2014). Oceanographic circulation
897 predicts low larval dispersal and observed genetic structure along a complex coastline. *Molecular*
898 *Ecology, 23,* 5036–5047. doi: 10.1111/mec.12924

899 Suyama, M., Torrents, D., & Bork, P. (2006) PAL2NAL: robust conversion of protein sequence
900 alignments into the corresponding codon alignments. *Nucleic Acids Research, 34*, W609-612. doi:
901 10.1093/nar/gkl315

902 Toonen, R. J., Puritz, J. B., Forsman, Z. H., Whitney, J. L., Fernandez-Silva, I., Andrews, K. R., &
903 Bird, C. E. (2013). ezRAD: a simplified method for genomic genotyping in non-model
904 organisms. *PeerJ*, *1*, e203.

905 Villinski, J. T., Byrne M., & Raff, R. A. (2002). Convergent maternal provisioning and life-history
906 evolution in echinoderms. *Evolution, 56,* 1764–1775. doi:10.1111/j.0014-3820.2002.tb00190.x

907 Wang, M., Uebbing, S., Pawitan, Y., & Scofield, D. G. (2018). RPASE: Individual-based allele-
908 specific expression detection without prior knowledge of haplotype phase. *Molecular Ecology*
909 *Resources*, *18*, 1247–1262. doi:10.1111/1755-0998.12909

910 Wang, Y., & Hey, J. (2010). Estimating divergence parameters with small samples from a large
911 number of loci. *Genetics, 184,* 363–379. doi:10.1534/genetics.109.110528

912 Waters, J. M., O'Loughlin, P. M., & Roy, M. S. (2004). Molecular systematics of some Indo-
913 Pacific asterinids (Echinodermata, Asteroidea): does taxonomy reflect phylogeny? *Molecular*
914 *Phylogenetics and Evolution, 30,* 872–878. doi:10.1016/j.ympev.2003.08.019

915 Weber, A. A. T., Merigot, B., Valiere, S., & Chenuil, A. (2015). Influence of the larval phase on
916 connectivity: strong differences in the genetic structure of brooders and broadcasters in the
917 *Ophioderma longicauda* species complex. *Molecular Ecology, 24,* 6080–6094.
918 doi:10.1111/mec.13456

919 Won, Y. J., & Hey, J. (2005). Divergence population genetics of chimpanzees. *Molecular Biology and*
920 *Evolution, 22,* 297–307. doi:10.1093/molbev/msi017

921
922

SUPPORTING INFORMATION

Appendix S1 DNA sequence alignments formatted as four input files for analysis in IMa2p

Appendix S2 IMa2p output from duplicate analyses of four data files (Appendix S1)

DATA ACCESSIBILITY

DNA sequence data can be accessed from the NCBI Sequence Read Archive under BioProjects PRJNA 544828 (*Cryptasterina*) and PRJNA 175319 (*Patiria miniata*).

AUTHOR CONTRIBUTIONS

Michael W. Hart designed the study, analyzed data, and wrote the paper.

Vanessa Guerra designed the study, analyzed data, and wrote the paper.

Maria Byrne contributed population samples and wrote the paper.

Jonathan B. Puritz designed the study and wrote the paper.

FIGURE LEGENDS

Figure 1 Three examples of gene genealogies that were analyzed in IMa2p models of divergence with gene flow between *Cryptasterina* spp. Gene names (and lengths of alignments) are contig names from the de novo transcriptome assembly. The alignment for each gene included six gene copies from one population sample of *C. pentagona* (blue), and eight gene copies from one population sample of *C. hystera* (orange). In each haplotype network the area of each symbol is proportional to its frequency in the alignment (from 1 to 8 occurrences in the total sample of 14 gene copies); black circles show nodes represented by unsampled haplotypes; numerals show the number of sequence differences between pairs of haplotypes when the value is greater than 1.

Figure 2 Posterior distributions of historical parameters from IMa2p models of divergence with gene flow between *Cryptasterina* species. In each plot the four curves show our new parameter value estimates based on duplicate analyses of datasets containing 999 loci from transcriptomes plus mtDNA (heavy lines) or 942 loci plus mtDNA (light lines). The high point of each curve indicates the maximum likelihood estimate (MLE) of the parameter value. The grey triangle shows the MLE from Puritz et al. (2012) based on few loci; the horizontal dotted line shows the 95% highest posterior density (HPD) estimate from our previous study; an arrow indicates a confidence interval from the previous estimate that was much wider than the priors (and the posteriors) in the new analyses in this study. Where the MLE or the HPD for the parameter values from Puritz et al. (2012) fell far outside the prior or the posterior distributions in this study, the previous estimate (and HPD) is shown in grey text. **(a)** Population divergence time (t). **(b)** Ancestral effective population size (N_{eA}).

Figure 3 Posterior distributions of effective population size (N_e) from IMa2p models of divergence with gene flow between **(a)** *Cryptasterina hystera* (orange) and **(b)** *C. pentagona* (blue). In each plot the four curves show our new parameter value estimates based on duplicate analyses of datasets containing 999 loci from transcriptomes plus mtDNA (heavy lines) or 942 loci plus mtDNA (light lines). The high point of each curve indicates the maximum likelihood estimate (MLE) of the parameter value. The grey triangle shows the MLE from Puritz et al. (2012) based on few loci; the horizontal dotted line shows the 95% highest posterior density (HPD) estimate from our previous study; an arrow indicates a confidence interval from the previous estimate that was much wider than the priors (and the

posteriors) in the new analyses in this study. Where the MLE or the HPD for the parameter values from Puritz et al. (2012) fell far outside the prior or the posterior distributions in this study, the previous estimate (and HPD) is shown in grey text.

Figure 4 Posterior distributions of immigration rates ($2N_em$) from IMa2p models of divergence with gene flow into **(a)** *Cryptasterina hystera* (orange) and **(b)** *C. pentagona* (blue). In each plot the four curves show our new parameter value estimates based on duplicate analyses of datasets containing 999 loci from transcriptomes plus mtDNA (heavy lines) or 942 loci plus mtDNA (light lines). The high point of each curve indicates the maximum likelihood estimate (MLE) of the parameter value. The grey triangle shows the MLE from Puritz et al. (2012) based on few loci; no confidence interval is shown for gene flow from our previous study, where we estimated that both gene flow parameters were not significantly different from zero by a likelihood ratio test.

Figure 5 Three examples of gene genealogies that were analyzed in IMa2p models of divergence with gene flow between populations of *Patiria miniata*. Gene names (and lengths of alignments) are contig names from the Pmin_1.0 reference genome assembly. The alignment for each gene included six gene copies from a northern population sample on Haida Gwaii (blue), and six gene copies from a southern population sample on Vancouver Island (orange). In each haplotype network the area of each symbol is proportional to its frequency in the alignment (from 1 to 3 occurrences in the total sample of 12 gene copies); black circles show nodes represented by unsampled haplotypes; numerals show the number of sequence differences between pairs of haplotypes when the value is greater than 1.

Figure 6 Posterior distributions of historical parameters from IMa2p models of divergence with gene flow between populations of *Patiria miniata*. In each plot the four curves show our new parameter value estimates based on duplicate analyses of datasets containing 999 loci from transcriptomes plus mtDNA (heavy lines) or 942 loci plus mtDNA (light lines). The high point of each curve indicates the maximum likelihood estimate (MLE) of the parameter value. The grey triangle shows the MLE from McGovern et al. (2010) based on few loci; the horizontal dotted line shows the 95% highest posterior density (HPD) estimate from our previous study; an arrow indicates a confidence interval from the previous estimate that was much wider than the priors (and the posteriors) in the new analyses in this study. Where the MLE or the HPD for the parameter values from McGovern et al. (2010) fell far outside the prior or the posterior distributions in this study, the previous estimate (and HPD) is shown in grey text. **(a)** Population divergence time (t). No value for the upper 95% HPD limit on divergence time is shown because in McGovern et al. (2010) we were not able to estimate an upper bound on the 95% HPD: the divergence time posterior was characterized by a mode at about 280,000 years, with a low but nonzero probability for much older divergence times that formed a long right-hand tail to the posterior and did not decline to zero. **(b)** Ancestral effective population size (N_{eA}). Note that in McGovern et al. (2010) we reported theta values (genetic diversity, not scaled for the mutation rate), not effective population sizes (scaled for the mutation rate). Here we show N_{eA} plotted on the same scale as our new estimates (relative to unscaled estimates of theta from our new data and analyses). For example, for the left-hand curve the MLE is N_{eA} ~6200 with theta~7.9; from McGovern et al. (2010) we estimated theta~7.0 (3.6-11.6), so on this scale the ancestral effective population size (and 95% HPD) in our previously published results was N_{eA}~5500 (2800-9100). Also note that in McGovern et al. (2010) we estimated that all three theta values in the model were not significantly different from each other by a likelihood ratio test.

Figure 7 Posterior distributions of effective population size (N_e) from IMa2p models of divergence with gene flow between **(a)** Vancouver Island (orange) and **(b)** Haida Gwaii (blue) populations of *Patiria miniata*. In each plot the four curves show our new parameter value estimates based on duplicate analyses of datasets containing 999 loci from transcriptomes plus mtDNA (heavy lines) or

942 loci plus mtDNA (light lines). The high point of each curve indicates the maximum likelihood estimate (MLE) of the parameter value. The grey triangle shows the MLE from McGovern et al. (2010) based on few loci; the horizontal dotted line shows the 95% highest posterior density (HPD) estimate from our previous study.

Figure 8 Posterior distributions of immigration rates ($2N_em$) from IMa2p models of divergence with gene flow into **(a)** Vancouver Island (orange) and **(b)** Haida Gwaii (blue). In each plot the four curves show our new parameter value estimates based on duplicate analyses of datasets containing 999 loci from transcriptomes plus mtDNA (heavy lines) or 942 loci plus mtDNA (light lines). The high point of each curve indicates the maximum likelihood estimate (MLE) of the parameter value. The grey triangle shows the MLE from McGovern et al. (2010) based on few loci; the horizontal dotted line shows the 95% highest posterior density (HPD) estimate from our previous study; an arrow indicates a confidence interval from the previous estimate that was much wider than the priors (and the posteriors) in the new analyses in this study. Where the MLE or the HPD for the parameter values from McGovern et al. (2010) fell far outside the prior or the posterior distributions in this study, the previous estimate (and HPD) is shown in grey text.